

# Techno-economic optimization of an energy system with sorption thermal energy storage in different energy markets

**Citation for published version (APA):**

Scapino, L., De Servi, C., Zondag, H. A., Diriken, J., Rindt, C. C. M., & Sciacovelli, A. (2020). Techno-economic optimization of an energy system with sorption thermal energy storage in different energy markets. *Applied Energy*, 258, [114063]. <https://doi.org/10.1016/j.apenergy.2019.114063>

**Document license:**  
CC BY

**DOI:**  
[10.1016/j.apenergy.2019.114063](https://doi.org/10.1016/j.apenergy.2019.114063)

**Document status and date:**  
Published: 15/01/2020

**Document Version:**  
Publisher's PDF, also known as Version of Record (includes final page, issue and volume numbers)

**Please check the document version of this publication:**

- A submitted manuscript is the version of the article upon submission and before peer-review. There can be important differences between the submitted version and the official published version of record. People interested in the research are advised to contact the author for the final version of the publication, or visit the DOI to the publisher's website.
- The final author version and the galley proof are versions of the publication after peer review.
- The final published version features the final layout of the paper including the volume, issue and page numbers.

[Link to publication](#)

**General rights**

Copyright and moral rights for the publications made accessible in the public portal are retained by the authors and/or other copyright owners and it is a condition of accessing publications that users recognise and abide by the legal requirements associated with these rights.

- Users may download and print one copy of any publication from the public portal for the purpose of private study or research.
- You may not further distribute the material or use it for any profit-making activity or commercial gain
- You may freely distribute the URL identifying the publication in the public portal.

If the publication is distributed under the terms of Article 25fa of the Dutch Copyright Act, indicated by the "Taverne" license above, please follow below link for the End User Agreement:

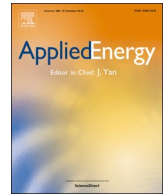
[www.tue.nl/taverne](http://www.tue.nl/taverne)

**Take down policy**

If you believe that this document breaches copyright please contact us at:

[openaccess@tue.nl](mailto:openaccess@tue.nl)

providing details and we will investigate your claim.



# Techno-economic optimization of an energy system with sorption thermal energy storage in different energy markets

Luca Scapino<sup>a,b,c,\*</sup>, Carlo De Servi<sup>a,c</sup>, Herbert A. Zondag<sup>b,d</sup>, Jan Diriken<sup>a,c</sup>, Camilo C.M. Rindt<sup>b</sup>, Adriano Sciacovelli<sup>e</sup>

<sup>a</sup> VITO NV, Energy Technology Unit, Thermal Systems Group, Boeretang 200, BE-2400 Mol, Belgium

<sup>b</sup> Eindhoven University of Technology, Department of Mechanical Engineering, P.O. Box 513, 5600MB Eindhoven, the Netherlands

<sup>c</sup> EnergyVille, Thor Park 8300, 3600 Genk, Belgium

<sup>d</sup> ECN Part of TNO, P.O. Box 15, 1755 ZG Petten, the Netherlands

<sup>e</sup> Birmingham Center for Energy Storage (BCES), School of Chemical Engineering, University of Birmingham, UK

## HIGHLIGHTS

- A sorption thermal energy storage is modeled in an optimization framework.
- A reference energy system operating in different market mechanisms is analyzed.
- The storage increased the system profits at the presence of balancing markets.
- Similarly, the market potential of other innovative technologies can be analyzed.

## ARTICLE INFO

### Keywords:

Sorption thermal energy storage  
Energy systems optimization  
Energy markets  
Mixed integer linear programming  
Organic Rankine cycle

## ABSTRACT

Sorption thermal energy storage (STES) has the potential to have higher energy densities and lower thermal losses compared to conventional thermal storage technologies, and it can contribute to increase the energy grid flexibility and the penetration of intermittent and distributed energy sources. However, STES is a technology still under research, and system-scale investigations are necessary to determine its potential in future energy systems. In this regard, the objective of this work is to investigate the STES potential in a reference energy system interacting with different energy markets. The system consists of a geothermal doublet supplying thermal energy to an organic Rankine cycle (ORC) and to a district heating network that satisfies the thermal energy demand of a residential neighborhood. A techno-economic optimization of the energy system is carried out using mixed integer linear programming. The optimization aims at finding the optimal STES size and system operational behavior that maximizes the yearly profits from selling the ORC energy to the energy markets. Among the main results, it is found that the STES integration increased the overall system profits by 41% in the scenario where the ORC interacted with the UK day ahead market (2017 data), and with two UK balancing services: the capacity market, and the short term operating reserve. In conclusion, this work highlights how a thermal storage technology still under research could become an asset under specific market conditions. Future policy mechanisms can benefit from similar analyses and foster the integration of new technologies into the energy grid.

## 1. Introduction

The increasing energy requirements of human society [1] and anthropogenic global warming [2] are among the main drivers for a transition towards sustainable energy systems, based on renewable energy sources such as solar and wind, in which anthropogenic CO<sub>2</sub> emissions are reduced [3]. The fluctuating nature of solar and wind will

require a higher degree of flexibility, in which energy production and usage can be spatially and temporarily decoupled. In this regard, thermal energy storage can be beneficial as thermal energy accounts for most of the final energy use in European households [4] and industry [5]. Different thermal storage solutions are nowadays studied whose storage capability can range from short-term to seasonal heat storage, and costs are competitive in the market [6].

\* Corresponding author at: VITO NV, Energy Technology Unit, Thermal Systems Group, Boeretang 200, BE-2400 Mol, Belgium.  
E-mail address: [l.scapino@tue.nl](mailto:l.scapino@tue.nl) (L. Scapino).

<https://doi.org/10.1016/j.apenergy.2019.114063>

Received 4 June 2019; Received in revised form 1 October 2019; Accepted 23 October 2019

Available online 22 November 2019

0306-2619/ © 2019 The Author(s). Published by Elsevier Ltd. This is an open access article under the CC BY license (<http://creativecommons.org/licenses/by/4.0/>).

**Nomenclature**

Symbol	Description [Unit]
$N_{STES}$	number of STES units [-]
$N_{dw}$	buildings number [-]
$R_g$	universal gas constant [J/(mol·K)]
$c_p$	specific heat capacity [J/(kg·K)]
$d_p$	particle diameter [m]
$\dot{m}$	mass flow [kg/s]
$p_{CM}$	capacity market price [€/kW·y]
$p_{STOR,AP}$	STOR market availability price [€/MW·h]
$p_w$	water vapor pressure [Pa]
$t_{sim}$	simulation timesteps [-]
$\varepsilon_{HR}$	heat recovery unit effectiveness [-]
$\Delta H_{react}$	reaction enthalpy [J/mol <sub>H<sub>2</sub>O</sub> ]
$\Delta S_{react}$	reaction entropy [J/(mol <sub>H<sub>2</sub>O</sub> ·K)]
RH	relative humidity [%]
z	objective function [€]
$\Delta p$	pressure losses [Pa]
AF	annuity factor [-]
C	cost [€]
E	energy [MWh]
IR	interest rate [-]
L	axial length [m]
M	molar mass [kg/mol]
NNPV	normalized net present value [-]
NPV	net present value [€]
P	power [MW]
R	revenues [€]
T	temperature [°C]
V	volume [m <sup>3</sup> ]
c	water vapor concentration [mol/m <sup>3</sup> ]
f	mass flow fraction [-]
lt	lifetime [years]
p	price [€/MWh]
t	time [s]
u	velocity [m/s]
$\varepsilon$	porosity [-]
$\eta$	efficiency [-]
$\mu$	viscosity [Pa·s]
$\nu$	stoichiometric coefficient [-]

 $\rho$  density [kg/m<sup>3</sup>]**Abbreviations**

CAPEX	capital expenditure
CM	capacity market
DAM	day ahead market
DHN	district Heating Network
HG	main heating grid
HR	heat recovery unit
HX	heat exchanger
LCOS	levelized cost of storage
MILP	mixed integer linear programming
OPEX	operating expense
ORC	organic Rankine cycle
STES	sorption thermal energy storage
STOR	short term operating reserve market

**Subscripts and superscripts**

a	air
amb	ambient
AP	availability price
cap	capacity
d	desorption
del	deliquescence
dry	drying
eq	equilibrium
fix	fixed
hum	humidification
max	maximum
min	minimum
reac	reaction
Res	residual
rt	return
s	sorption
sat	saturated
sl	salt
sp	supply
UP	utilization price
v	water vapor

Given the current evolution of energy systems, the future energy grid will arguably consist of different energy conversion units, mostly non-dispatchable. The assessment of the most promising storage technologies entails thorough techno-economic analyses and optimization studies, encompassing different operating scenarios and remuneration schemes for the energy suppliers. Techno-economic analyses and optimization studies have been already applied to multi-energy systems, and mixed integer linear programming (MILP) has been widely used as optimization approach. The MILP approach, as other optimization approaches, aims at minimizing or maximizing an objective function by selecting the value of the optimization variables, which are also bounded by optimization constraints. For instance, studies investigated the capability of the energy network at a country-level to deal with the coexistence of intermittent production sources and cogeneration plants [7]. Micro-grids as stand-alone systems [8], interacting with the main grid [9], and their ability to provide market services such as reliability and flexibility [10] have also been studied within a MILP framework. Concerning electrical storage, different battery technologies have been investigated for community energy storage and market service provision [11] or for profit maximization of renewable energy systems [12]. Regarding thermal energy storage, the conversion of electricity into

heat and cold energy to increase grid flexibility has been studied [13]. Finally, also the integration of seasonal heat storage at district level has been investigated for increasing the amount of renewable heat supply [14].

Although heat storage is expected to have an important role in these future optimized energy systems, the future potential of advanced thermal energy storage (TES) technologies such as latent [15] or sorption [16] heat storage in different systems and market scenarios has not yet been extensively investigated. The main reason thereof is that the technology readiness level (TRL) of these technologies is relatively low, and several scientific challenges still need to be overcome. Concerning sorption thermal energy storage (STES), which is based on storing thermal energy in a reversible reaction, the main challenges are still at material- and prototype-scale. In particular, suitable materials with, among the main requirements, a sufficiently high energy density, stability, and cyclability are still a matter of research. Salt hydrates [17], pure adsorbents such as zeolites [18], silica gel [19], aluminophosphates and silico-aluminophosphates [20], metal organic frameworks [21], and composite materials [22] are being thoroughly investigated to find promising candidates that meet the abovementioned conditions. Moreover, challenges at prototype-scale such as

improvement of heat and mass transfer in sorption reactors [23] and prevention of components corrosion [24] are also under investigation. However, beside the extensive research at material- and prototype-scale, techno-economic analyses involving sufficient technological knowledge are crucial to have consistent and physics-based insights that, in turn, can lead to the optimal integration of new technologies in future energy systems. For instance, these analyses can provide essential insights required for the creation of favorable market conditions by policy makers and market stakeholders. This is especially true for technologies that are still under development, with a low TRL, or that have a niche market.

In light of this, the aim of this work is to investigate, within a MILP framework, the economic impact of an open solid sorption thermal energy storage in a reference energy system that operates in different energy markets. The reference energy system is inspired by an existing installation in Belgium and consists of a main heating grid (HG) that extracts the thermal energy from a geothermal doublet, and supplies it to a low temperature district heating network (DHN) and an organic Rankine cycle (ORC). The impact of a STES on the energy system yearly profit is assessed for different storage sizes in the presence of different market mechanisms. The electricity markets considered in this work are the Belgian day ahead market (2013 data), and the UK market (2017 data). The Belgian market has been selected because the location of the existing geothermal doublet is in Belgium. The additional investigation on the UK market has been carried out due to the presence of various balancing services that could make the integration of energy storage profitable.

Two main contributions are present within this manuscript. The first contribution is a STES formulation within the MILP framework taking also into account the specific technological aspects of this storage type. The second contribution is an assessment of the economic benefits of adding an innovative thermal storage technology within different economic frameworks. Sorption heat storage is a technology still under research. Therefore, it is essential to understand its future competitiveness in the energy network and to focus the scientific research on the most critical issues and main challenges for the integration of this technology in the market. In particular, this work investigates the benefits of a STES for an energy producer to operate simultaneously in different energy markets, i.e. the retail market and balancing services, in order to maximize the yearly profits.

The current work is divided into six main sections (Fig. 1.1). Section 2 introduces the reference energy system (2.1), the energy markets (2.2), and the different scenarios investigated in this work (2.3). Section 3 focuses on the modelling methodology and describes the different system components, with special focus on the STES. Section 4 presents the optimization framework by introducing the optimization variables

(4.1), the objective function and the problem optimization constraints (4.2). Section 5 presents the results of the analysis. First, the major highlights and results overview for all the scenarios are shown (5.1). Then, each scenario in which the STES is included in the optimal solution is individually addressed and discussed (5.2–5.4). Finally, in Section 6, the main conclusions of this work are presented.

## 2. Reference energy system

In this section the main components of the reference energy system are described (2.1). Then, the energy market mechanisms that are being investigated are defined (2.2) and the different scenarios in which the reference energy system is operating are shown (2.3).

### 2.1. General description

In this section, a general overview of the reference energy system is presented. The details and assumptions about every system component are given in Section 3. The reference energy system and the interaction between the different components is displayed in Fig. 2.1. The system consists of a deep geothermal doublet delivering thermal energy to a main medium-temperature heating grid (HG) with a supply temperature of 114 °C. Two main consumers are connected. The first consumer is a low-temperature district heating network (DHN) with a supply temperature of 55 °C, supplying a neighborhood with thermal energy for space heating and domestic hot water, which has priority as heat consumer. In Section 3 (Table 3-1), the single energy system components are described more in detail. The second consumer is an organic Rankine cycle (ORC), which can produce electricity from the remaining fraction of mass flow in the geothermal plant that is not used for providing the demand of the DHN. Within this energy system, a STES consisting of several modular units is integrated. The STES size (the number of modular units) is varied in order to find the optimal STES size for every scenario that maximizes the yearly system profit. A key point of this work is to investigate the impact of different energy markets, in which the reference energy system is operating. Different market mechanisms can provide additional revenues and make the use of the STES more or less profitable. The aim of the optimization is to assess the optimal STES size and its role as flexibility provider while maximizing the overall system profit during a year of operation and respecting the main system constraints such as guaranteeing the energy provision to the DHN. At every moment in time, part of the energy from the main heating grid can be used to satisfy the thermal energy demand from the DHN ( $f_{DHN}$ ), for the electricity production with the ORC ( $f_{ORC}$ ), or for charging (desorption) the STES ( $f_{STES}$ ). The STES could partially satisfy the DHN demand when the ORC is making high

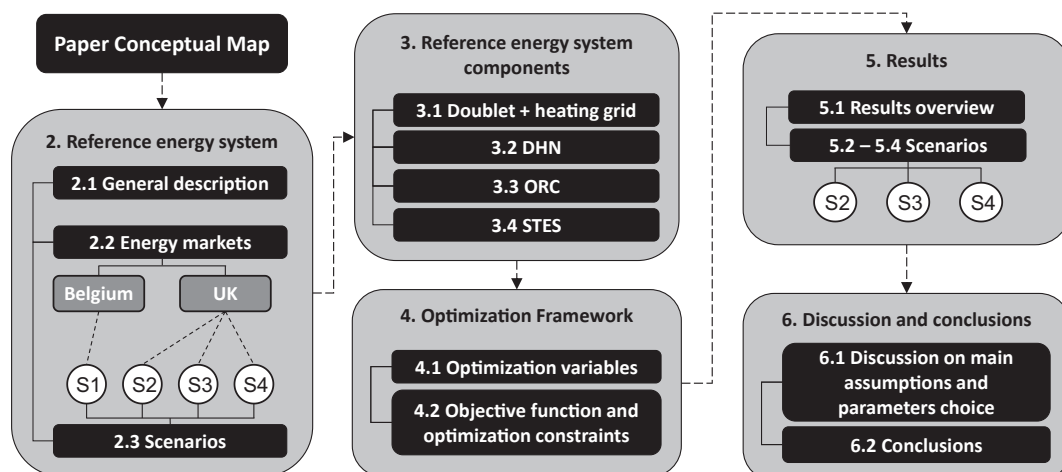


Fig. 1.1. Conceptual map of the manuscript structure.

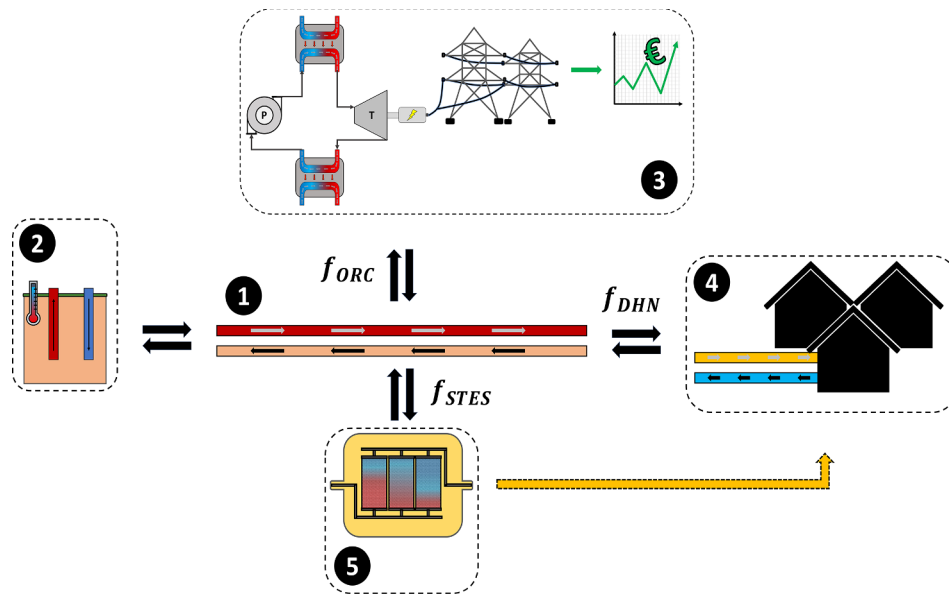


Fig. 2.1. Top: Reference Scenario. 1: Main heating grid (HG). 2: Geothermal doublet. 3: Organic Rankine cycle. 4: Low temperature district heating network (DHN). 5: Sorption thermal energy storage (STES).

revenues in selling electrical power to the energy markets. Therefore, the mass flow fraction used by the ORC to produce electrical power at a specific moment can be increased. The optimization problem consists of selecting the water mass flow fractions from the heating grid to the three energy consumers ( $f_{DHN}$ ,  $f_{ORC}$ ,  $f_{STES}$ ) at every time step.

## 2.2. Energy markets

Energy markets and balancing services are numerous and differ among countries and among each other in terms of availability in time, remuneration schemes, and technical requirements of the electricity producers to operate in a specific market. Among the typical technical requirements for an electricity producer there is the minimum installed capacity, a minimum delivery time during which the committed capacity has to be constantly delivered, and the generator response time. The latter, for a balancing service, is a crucial parameter. Balancing services for the grid frequency control require response times typically within one second while services for fast reserve of active power typically require response times in the order of few minutes.

In this work, several energy market mechanisms in Belgium and UK have been considered. The reason why the Belgian market has been selected is that the deep geothermal doublet is inspired by an existing installation in Mol (BE). Moreover, the aggregated thermal energy demand profile of the DHN represents an existing urban district located in Genk (BE). For the investigated Belgian market, the data from 2013 have been used due to their availability. The reason why the UK region has been selected is that in UK there are various balancing market mechanisms that remunerate the energy producers with additional or higher revenue streams for the provision of flexibility. For the UK markets investigated in this work, the most recent available data (2017) have been used.

Three main market mechanisms are investigated. The day ahead market (DAM), a market that is always active, in which the electricity price is set according to the forecasted energy demand and production; the capacity market (CM), a UK compensation mechanism based on the yearly committed capacity of a generation unit that has to be available during stressful events (e.g. unforeseen availability of a producer); and the short term operating reserve (STOR), a UK balancing service that is used to fill the gap between the forecasted demand required by the grid and the actual demand. In this work, when multiple market mechanisms are active in the same scenario, the ORC can sell the energy to all

of them.

### 2.2.1. Day ahead market (DAM)

The day ahead market is a traditional market mechanism in which consumers and producers establish the electricity price one day ahead of the delivery. Within this market, the ORC can sell electricity with the principle of tariff arbitrage. Therefore, the ORC tries to sell as much electricity as possible when the price  $p_{DAM}$  is high.

### 2.2.2. Capacity market (CM)

The Capacity Market (CM) [25] is a mechanism that provides a predictable yearly revenue stream for a generation unit. The generation unit is compensated for committing its capacity to the national grid for a predefined amount of years. In exchange for the yearly compensation, the unit is committed to generate during stressful grid events (CM-event), otherwise penalties are faced. A stressful event might arise due to e.g. an unforeseen availability of a generator, and the national grid might not have sufficient production resources to fulfill the forecasted demand, already including other balancing services. There has not been a CM-event since 2016 in the UK grid [26]. Within this work, the clearing price ( $p_{CM}$ ) of the 2016 CM market auction is used [27], 22.5 €/kW-year, and shown in Table 2-1. Moreover, a CM-event is imposed into the optimization model on January 5th. In this work, the revenues from the CM market depend on how much power the ORC delivers to an energy market during the CM-event. For example, if during the CM-event, the ORC produces an electric power of 1 MW and sells the energy to a market (DAM or STOR), an additional yearly revenue stream of 22,500 € is produced.

### 2.2.3. Short term operating reserve (STOR)

The Short Term Operating Reserve (STOR) [28] is a balancing service used in UK at certain times of the day in order to provide extra

Table 2-1 Short term operating reserve and Capacity market parameters.

Parameter	Value	Unit
$p_{CM}$	22.5	€/kW-year
$p_{STORAP}$	4.76	€/MWh
$p_{STORUP}$	168.64	€/MWh

capacity in case that the forecasted electricity demand is higher than the actual demand or in case of unforeseen unavailability of generators. The service is typically active during two time windows of the day to address the morning and evening peaks. The time interval of each window can vary depending on whether it is a business or weekend day. Moreover, the availability windows vary over the year according to six periods, hereafter referred as “STOR seasons”. Currently, this market is open to generators with a capacity of 3 MW or larger. However, aggregated contracts can be possible, and lower capacity units can operate together to meet the minimum capacity requirement. The compensation system of the STOR balancing service consists of two parts. The generator is compensated, with an availability price ( $p_{STORAP}$ ), for committing a certain capacity to the service, even if it is not used. Moreover, in case the generator is called to generate, it will be compensated, with a utilization price ( $p_{STORUP}$ ), for the generated electricity. In this work, the average availability and utilization prices for 2017 are used [29] and shown in Table 2-1. It has to be remarked that the availability price ( $p_{STORAP}$ ) compensates the producer for the committed power in every time window (i.e. €/ (MW·h)) while the utilization price ( $p_{STORUP}$ ) compensates the producer for the energy effectively sold in a time window (i.e. €/ (MWh)).

The optimization model in this work is a deterministic model. Therefore, a utilization profile of the generation unit has to be known *a priori*. In order to do so, a probability to generate is calculated for every time window based on the amount of days present in the STOR season and the amount of days in which the service has been effectively used by the electricity grid in that STOR season [29]. With that, a probability-based generation profile for the STOR service is produced. In this work, it is assumed that the generator (ORC) is always able to provide the committed capacity to the STOR market. However, in a real case scenario, there might be energy delivery failures from an energy producer due to various reasons (i.e. technical issues).

### 2.3. Scenarios

The reference energy system presented in Section 2.1 is investigated with different scenarios (Fig. 2.2). For every scenario, the amount of sorption reactor segments is varied and the impact on the overall system profit is assessed. The first two scenarios, S1 and S2, assume that the reference energy system can operate only in the day ahead market (DAM) and sell energy with a strategy based on tariff arbitrage. The STES integration could be beneficial for the ORC to produce more electricity when prices on the DAM are higher. This would allow the main heating grid to allocate more mass flow for the ORC electricity production and satisfy the DHN demand by discharging the STES. Scenarios S3 and S4 include additional balancing services in which the ORC can operate, in the UK market. Scenario S3 assumes that the generation unit can also operate in the capacity market. In this scenario, the ORC could maximize its committed capacity during grid stressful events thanks to the STES presence. Finally, S4 adds also the STOR market among the possible balancing services in which the ORC can operate. Being a market available only during certain time windows of the day, the STES integration could allow the ORC to maximize its energy production during those time periods.

## 3. Reference energy system components

In this section, the main system components are described individually. In Section 3.1, the relevant information is presented on the deep geothermal doublet and on the main heating grid, operating at medium-temperature. In Sections 3.2 and 3.3, the low temperature district heating network and ORC are described, respectively. Finally, in Section 3.4, the STES main concepts and operational behavior are described in detail. In Table 3-1, the main parameters of the energy systems components are shown.

### 3.1. Geothermal doublet and heating grid

The deep geothermal doublet and main heating grid relevant parameters are based on an existing installation in Mol, Belgium [30]. It is assumed that the doublet will deliver a fixed thermal power at a constant temperature of 125 °C throughout the whole year. Due to this assumption, in the modeling framework, the doublet will not be directly simulated. The thermal energy is then transferred to a heating grid through a heat exchanger in which the heating grid supply ( $T_{HG,sp}$ ) and return temperatures ( $T_{HG,r}$ ) are 114 °C and 70 °C, respectively, and a fixed mass flow ( $\dot{m}_{HG}$ ) of 161 kg/s is used (Table 3-1).

### 3.2. Low temperature district heating network (DHN)

A 4th generation district heating network [31] has been assumed in the reference scenario. It is defined as a thermal energy system able to satisfy the thermal energy needs of low energy buildings with low temperature heat sources. In terms of operating temperatures, a supply temperature ( $T_{DHN,sp}$ ) of 55 °C and a return temperature ( $T_{DHN,r}$ ) of 30 °C have been assumed (Table 3-1). The DHN thermal energy demand,  $P_{DHN}$ , has been inspired from an urban district in Genk (BE), consisting of approximately seven thousand buildings (Fig. 3.1). A tool based on the work of Remmen et al. [32] and De Jaeger et al. [33], available also in van der Heijde [34], which includes building models taking into account the building type (detached, semi-detached, terraced), geometry and the year of construction, together with a stochastic occupancy model [35], has been used to estimate the aggregated demand of the abovementioned urban district. For this work, the aggregated profile has been scaled down so that the DHN thermal energy demand can be satisfied in every period of the year with the assumed mass flow rate of the main heating grid ( $\dot{m}_{HG}$ ), leading to a maximum deliverable power of approximately 29.65 MW and corresponding to the maximum heating demand of approximately 1200 dwellings. Based on the stochastic occupancy model, the heating temperature set point can vary within the interval between 15 °C and 20 °C. The DHW demand supply temperature at the building level is assumed at 55 °C and the mains temperature at 10 °C. The heating demand has been determined using the data from a typical meteorological year from a weather station of Uccle (BE), representative for the Belgian climate. It has to be remarked that the typical meteorological year does not represent a specific year, but it is the result of using historical data to produce typical conditions for 12 representative months [36]. Therefore, in this work, the heating demand is based on the typical meteorological year data, while the price signals are specific for one year (2013 for Belgium and 2017 for UK).

### 3.3. Organic Rankine cycle

An ORC model, in which a cooling tower is used to remove the heat from the condenser water, has been used to estimate the net electric power  $P_{ORC}$  produced given three main input parameters: the available

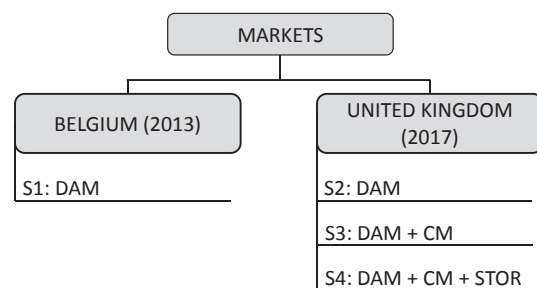


Fig. 2.2. Scenarios investigated and active market mechanisms present in each scenario. DAM = day ahead market. CM = capacity market. STOR = short term operating reserve.

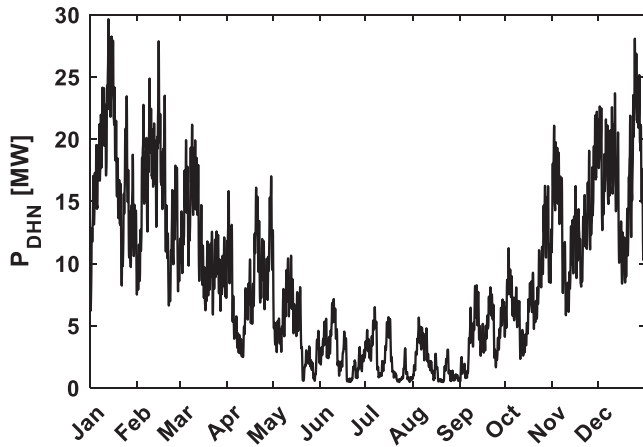


Fig. 3.1. Aggregated thermal energy demand of the investigated low temperature district heating network.

mass flow fraction from the heating grid  $f_{ORC}$  at  $T_{HG,sp}$ , which determines the amount of ORC fluid that can be evaporated; the temperature  $T_{amb,t}$  and humidity  $RH_{amb,t}$  of the ambient air, which determine the performance of the cooling tower and, consequently, also the power required from the auxiliary systems such as the cooling tower fan and condenser water pump. The model has as main inputs several assumptions and technological constraints inspired by a project under development in Mol (BE) [30]. The modeled ORC consists of a sub-critical Rankine cycle with propane as organic fluid and a nominal power of 2.5 MW. The ORC fluid properties and thermodynamic states were estimated with CoolProp [37] while the design guidelines and components sizing have been done according to Sinnott [38]. It is assumed that the ORC can operate with a minimum evaporator mass flow ( $f_{ORC,min}$ ) of 20% of the nominal one, and that the return temperature of the evaporator is fixed at  $T_{HG,r}$ . Regional weather data from 2007 to 2016 have been used to define the operating boundaries of the ORC in terms of relative humidity and temperature of ambient air. Then, the off-design net power produced at every possible weather condition and evaporator mass flow has been mapped. In Fig. 3.2 left, the net power delivered at three different evaporator mass flows is shown. In Fig. 3.2 right, the net power delivered at four different temperature and humidity levels is displayed. At low ambient temperature and humidity, the cooling tower is able to minimize the condenser water temperature, resulting in higher enthalpy difference in the ORC turbine, and therefore in higher produced power. Vice versa, at higher temperature and humidity, the ORC condensation temperature is increased, and the ORC fluid enthalpy difference exploited in the ORC turbine is lower resulting in a lower net power produced. For certain conditions, the auxiliary

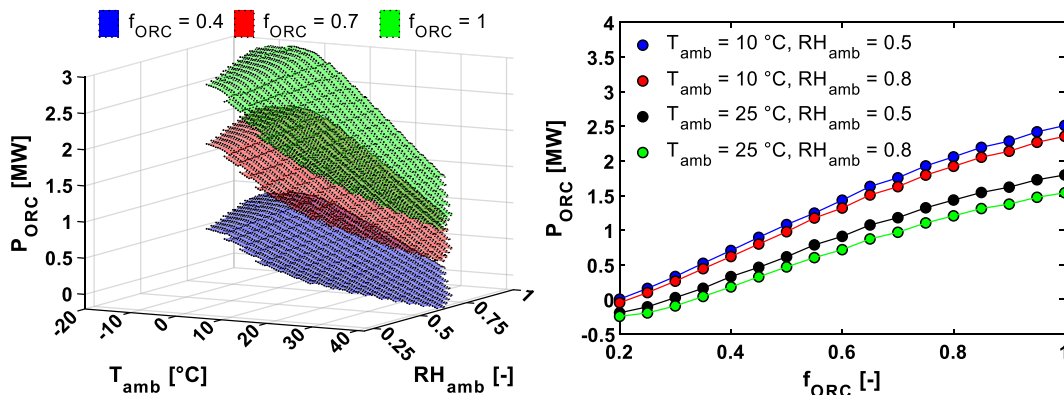
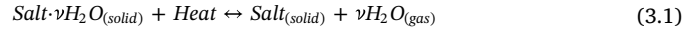


Fig. 3.2. Net power of the ORC and cooling towers system in function of ambient temperature and humidity, and mass fraction from the main heating grid directed to the ORC evaporator ( $f_{ORC}$ ). Left: Net power production for three different mass fractions. Right: Net power production in function of the mass fraction  $f_{ORC}$  at four fixed ambient temperature and humidity levels.

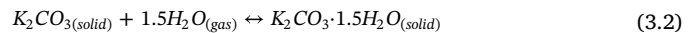
power required is greater than the power produced by the turbine, resulting in a negative net power delivered from the system.

### 3.4. Sorption thermal energy storage

Sorption thermal energy storage (STES) is based on storing thermal energy in a material made at least by two components: a sorbent (e.g. salt hydrates, silica gel, zeolites) and a sorbate (e.g. water vapor). The two components participate in a reversible reaction in which thermal energy can be stored within the chemical and physical bonds of the material. In Eq. (3.1) an example is presented of a reversible reaction for a general salt hydrate/ $H_2O$  system, in which  $\nu$  is the  $H_2O$  stoichiometric coefficient.



During the sorption phase (exothermic reaction), the sorbent and the sorbate are combined and heat is released. Vice versa, during the desorption phase (endothermic reaction), heat is needed in order to separate the sorbent and the sorbate. STES systems can be divided into two main categories from the layout perspective: open and closed systems. An open system allows mass and energy to be exchanged with the environment, and it is relatively less complex than a closed system in terms of required components. Moreover, it operates at atmospheric pressure and the heat can be efficiently extracted or injected into the system by forced circulation of the airflow. However, auxiliary energy is necessary in order to drive the airflow with a fan through the packed bed and overcome the pressure losses. Moreover, a nontoxic material must also be selected since it is in direct contact with the environment. More information on the main advantages and drawbacks of open and closed STES systems can be found in Scapino et al. [39]. In this work, a salt hydrate/ $H_2O$  open solid sorption system is considered, in which the porous material (sorbent) is stored in cylindrical packed beds and the sorbate is transported by an air flow. In particular, the salt hydrate properties of potassium carbonate are used in this work. Potassium carbonate has been identified as possible candidate for STES as a result of an extensive screening process [17] and an in-depth investigation accounting also for the material stability and cyclability [40]. This sorption material has a reversible reaction from anhydrous to sesquihydrate, displayed in Eq. (3.2). The estimated reaction crystal energy density is 1.3 – 1.4  $GJ/m^3$  [17,41].



In Fig. 3.3, the equilibrium temperature and deliquescence [42] lines for the selected material, together with the water saturation line are shown. For a water vapor pressure of e.g. 1200 Pa, corresponding approximately to saturated air at 10 °C, an equilibrium temperature of approximately 60 °C would occur.

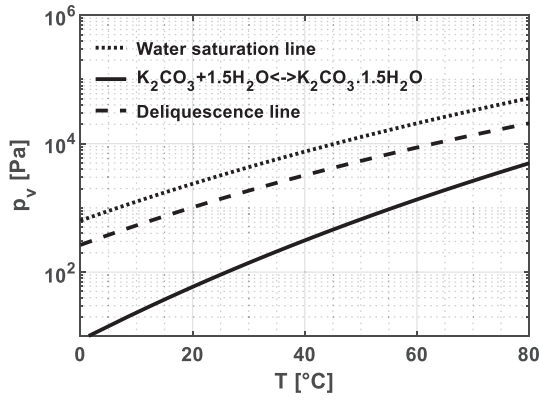


Fig. 3.3. Equilibrium curve for  $K_2CO_3 + 1.5H_2O \leftrightarrow K_2CO_3 \cdot 1.5H_2O$  (solid line), deliquescence line [42] (dashed line), and water vapor saturation line (dash-dotted line).

During desorption (Fig. 3.4, top), warm air is flushed into the reactor and separates the water molecules from the porous material. As a result, a colder and more humid airflow exits from the system. During sorption (Fig. 3.4, bottom), water vapor in the cold and humid airflow flushing the reactor produces an exothermic reaction with the porous material, and warm and drier air exits from the system.

The STES is connected to both the heating grid HG and the low temperature district heating network DHN as shown in Fig. 3.5. An air/water heat exchanger (HX1) connects the main heating grid to the storage in order to provide the necessary thermal energy for the desorption phase (i.e. storage charging). A second air/water heat exchanger (HX2) connects the storage to the low temperature heating network, for the sorption phase (storage discharging). In this work, it is assumed that both heat exchangers can transfer the useful heat up to a minimum temperature difference between the two fluids of  $\Delta T_{min,HX} = 1^\circ C$ . A heat recovery (HR) with a rated efficiency  $\varepsilon_{HR}$  of 90% [44] is assumed in order to preheat the inlet air with the storage exhaust air. During the desorption phase (red line), the valves V1 and V2 direct the preheated airflow of state 2 towards the heat exchanger from the main heating grid (3<sub>d</sub>), and valve V3 and V4 direct the airflow towards the heat recovery unit bypassing the DHN heat exchanger. During the sorption phase (blue line), the valves V1 and V2 bypass the heat exchanger used for the desorption phase (HX1) and direct the flow from the heat recovery unit towards the inlet of the reactor (3<sub>s</sub>). Valve V3 directs the flow towards the heat exchanger for the low temperature DHN (4<sub>s</sub>). In both sorption and desorption phases, the heat recovery unit preheats the inlet airflow with the waste heat remained after the thermal load (sorption phase) or the reactor desorption. Finally, only during sorption, the ambient

airflow can be mixed with saturated air through valve V6 or mixed with the exhaust dry air through valves V5a and V5b (blue-black dashed lines). This is done, in order to prevent the sorption material deliquescence and to guarantee, where possible, a minimum temperature lift in the sorption reactor. A more extensive discussion regarding this is present in the next paragraphs. The sorption reactor is divided conceptually into a set of units, or cylindrical segments ( $N_{STES,tot}$ ). The segments are supposed to work in a parallel configuration in which every segment can be active or inactive. Therefore, if multiple segments are active at a certain timestep, they will be exposed to the same operating conditions in terms of airflow, inlet temperature and sorbate concentration. The main objective of the STES model is to quantify the charging ( $P_{STES-d,unit,t}$ ) and discharging ( $P_{STES-s,unit,t}$ ) power required by every STES unit depending on the sorption material characteristics, the reactor main parameters, the ambient conditions and the technological characteristics of other system components such as the heat recovery unit.

The preheated reactor inflow air temperature during sorption ( $T_{2s}$ ) can be calculated according to Eqs. (3.3) and (3.4).

$$T_{3s,t} = T_{2,t} = T_{1,t} + \varepsilon_{HR}(T_{3s} - T_{1,t}) \quad (3.3)$$

$$T_{3s} = T_{DHN,rt} + \Delta T_{min,HX} \quad (3.4)$$

where  $T_{1,t}$ ,  $T_{3s}$  and  $T_{DHN,rt}$  are the airflow temperatures at the inlet of the heat recovery unit and after the thermal load, and the DHN return temperature of the water, respectively. The temperature lift achieved from the exothermic reaction ( $\Delta T_{react,t}$ ) and the reactor outlet temperature ( $T_{4s,t}$ ), are estimated assuming that all the reaction energy is used to heat up the air flow, and that the outlet temperature cannot exceed the reaction equilibrium temperature ( $T_{eq-s,t}$ ), according to Eqs. (3.5)–(3.7).

$$T_{4s,t} = \min(T_{3s,t} + \Delta T_{react,t}, T_{eq-s,t}) \quad (3.5)$$

$$\Delta T_{react,t} = \frac{c_{3s,t} \Delta H_{react}}{\rho_a c_{p,a}} \quad (3.6)$$

$$T_{eq-s,t} = \frac{-\Delta H_{react}}{-\Delta S_{react} - R_g \ln\left(\frac{1}{p_{v,3s,t} c_{3s,t}}\right)} \quad (3.7)$$

where  $\Delta H_{react}$  and  $\Delta S_{react}$  are the enthalpy and entropy of reaction per mole of water, respectively.  $R_g$  is the ideal gas constant,  $p_{v,3s,t}$  the water vapor pressure in the airflow at time  $t$ , and  $c_{3s,t}$  the water vapor molar concentration. The inlet water vapor concentration has been calculated for the whole year from the weather data ( $T_{amb,t}$  and  $RH_{amb,t}$ ). Moreover, a lower and upper limit are assumed for  $c_{3s}$  in order to achieve a minimum temperature lift ( $\Delta T_{react,t}$ ) and to prevent the sorption material deliquescence, respectively. In order to prevent that the sorbent material faces deliquescence due to too high values of sorbate concentration,

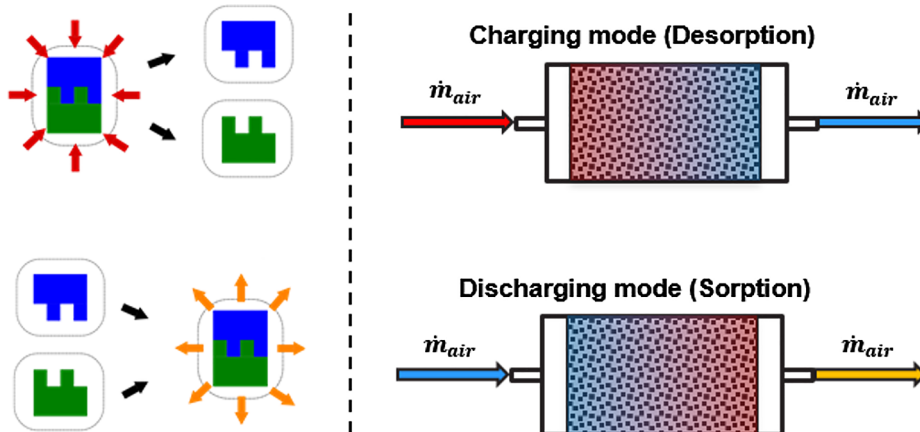


Fig. 3.4. Sorption reactor concept [43]. Top: Desorption phase. Bottom: Sorption phase.

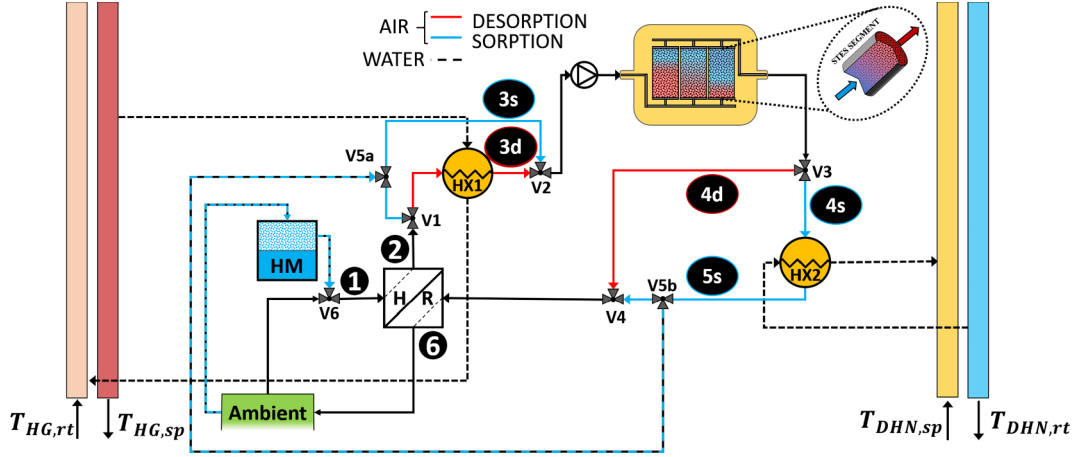


Fig. 3.5. Sorption thermal energy storage system integrated into the reference energy system. HM = humidification. HR = heat recovery.  $T_{HG,sp} = 114\text{ }^{\circ}\text{C}$ .  $T_{HG,rt} = 70\text{ }^{\circ}\text{C}$ .  $T_{DHN,sp} = 55\text{ }^{\circ}\text{C}$ .  $T_{DHN,rt} = 30\text{ }^{\circ}\text{C}$ .

an upper limit has been imposed ( $c_{max,t} = 0.95c_{del,t}$ ) for the water vapor concentration. The limit is based on the sorbate concentration that would cause the sorbent material deliquescence ( $c_{del,t}$ ), which is a function of the ambient relative humidity, based on the work of Greenspan et al. [42]. If, at specific times of the year, the ambient air would have a higher water vapor concentration than  $c_{del,t}$ , then it is mixed with part of the exhaust air at  $T_{5s}$ , assumed dry, with a mixing ratio  $X_{dry,t}$ . The exhaust air is assumed to be extracted before entering in the heat recovery unit, and it is mixed with the ambient airflow after the heat recovery unit. Counter wise, in order to guarantee a minimum amount of sorbate concentration in the airflow during sorption, it is also assumed that saturated air at a temperature  $T_{hum}$  of  $10\text{ }^{\circ}\text{C}$  is available. Therefore, providing that the maximum sorbate concentration  $c_{max,t}$  is not exceeded, the incoming airflow can be humidified with a mixing ratio  $X_{hum,t}$  up to a maximum water vapor concentration of  $c_{sat,10\text{ }^{\circ}\text{C}} = c(T = 10\text{ }^{\circ}\text{C}, RH = 100\%)$ . This could be achieved, for example, by recovering part of the low temperature heat from the ORC cooling tower. Therefore, the concentration at every time step  $t$  of the year follows Eq. (3.8).

$$c_{3s,t} = \min(\max(c_{sat,10\text{ }^{\circ}\text{C}}, c_{amb,t}), c_{max,t}) \quad (3.8)$$

If air humidification occurs, then the incoming airflow temperature is calculated according to Eq. (3.9). Alternatively, if mixing with dry exhaust occurs, the resulting airflow temperature entering in the reactor ( $T_{3s,t}$ ) is adjusted according to Eq. (3.10).

$$T_{1,t} = T_{hum}X_{hum,t} + (1 - X_{hum,t})T_{amb,t} \quad (3.9)$$

$$T_{3s,t} = X_{dry,t}T_{5s} + (1 - X_{dry,t})T_{2,t} \quad (3.10)$$

Here,  $T_{2,t}$  is the temperature of the ambient air at the outlet of the heat recovery unit and  $T_{5s}$  is the exhaust air from the STES, after the thermal load. The thermal power from one STES unit discharge process ( $P_{STES-s,unit,t}$ ) can be calculated according to Eq. (3.11), with  $\dot{m}_a$  and  $c_{p,a}$  the air mass flow and specific heat capacity, respectively.

$$P_{STES-s,unit,t} = \dot{m}_a c_{p,a} (T_{4s,t} - T_{3s,t}) \quad (3.11)$$

In Eq. (3.11),  $T_{4s,t}$  and  $T_{3s,t}$  are the airflow temperatures at the inlet and outlet of the heat exchanger transferring the heat to the thermal load (HX2). The STES discharging efficiency  $\eta_{STES-s}$ , defined as the amount of thermal power effectively transferred to the DHN, can be defined as in Eq. (3.12).

$$\eta_{STES-s,t} = \frac{T_{4s,t} - (T_{DHN,rt} + \Delta T_{min,HX})}{T_{4s,t} - T_{3s,t}} \quad (3.12)$$

The energy transferred to the DHN water through the heat exchanger HX2 is calculated with Eq. (3.13).

$$P_{STES-DHN,unit,t} = \eta_{STES-s,t} P_{STES-s,unit,t} \quad (3.13)$$

Finally, after the thermal load, the residual thermal energy in the airflow after the heat exchanger HX2 (at  $T_{5s}$ ), is used in the heat recovery unit to preheat the incoming airflow (Eq. (3.3)). Similarly, during the desorption phase, the inlet hot air temperature in the heat recovery unit corresponds to the outlet temperature of the reactor during desorption, which in turn is equal to the reaction equilibrium temperature ( $T_{4d,t} = T_{eq-d,t}$ ). Thus, the preheated ambient air temperature ( $T_{2d,t}$ ) can be estimated with Eq. (3.14).

$$T_{2d,t} = T_{1,t} + \varepsilon_{HR} (T_{4d,t} - T_{1,t}) \quad (3.14)$$

$$T_{3d} = T_{HG,sp} - \Delta T_{min,HX} \quad (3.15)$$

The preheated ambient air ( $T_{2d,t}$ ) is heated up to the temperature  $T_{3d}$  (Eq. (3.15)) in the heat exchanger HX1 from the main heating grid (HG) supply water flow at  $T_{HG,sp}$ . The water vapor concentration present in the air corresponds to the one at ambient conditions ( $c_{1,t}$ ). In the desorption phase, there is no risk of material deliquescence nor a minimum concentration value has to be achieved. Therefore, minimum and maximum concentration limits are not required. The useful desorption energy for charging the STES ( $P_{STES-d,unit,t}$ ) is only the one released above the reaction equilibrium temperature ( $T_{eq-d,t}$ ), assuming that all the heat above  $T_{eq-d,t}$  is absorbed in the reactor. Similar to the sorption phase, the desorption energy transferred from the heating grid (HG) to the airflow ( $P_{STES-HG,unit,t}$ ) can be calculated according to Eqs. (3.16)–(3.19).

$$T_{eq-d,t} = \frac{-\Delta H_{reac}}{-\Delta S_{reac} - R \ln \left( \frac{1}{p_{v,3d,t}(T_{3d}, c_{1,t})} \right)} \quad (3.16)$$

$$P_{STES-d,unit,t} = \dot{m}_a c_{p,a} (T_{3d} - T_{eq-d,t}) \quad (3.17)$$

$$\eta_{STES-d,t} = \frac{T_{3d} - T_{eq-d,t}}{T_{3d} - T_{2d,t}} \quad (3.18)$$

$$P_{STES-HG,unit,t} = \frac{P_{STES-d,unit,t}}{\eta_{STES-d,t}} = \dot{m}_a c_{p,a} (T_{3d} - T_{2,t}) \quad (3.19)$$

The maximum amount of energy that can be stored in one STES unit ( $E_{STES,unit}$ ) can be calculated with Eq. (3.20).

$$E_{STES,unit} = \frac{(1 - \varepsilon) \rho_{sl} V_{STES,unit} \nu \Delta H_{reac}}{M_{sl}} \quad (3.20)$$

where  $\varepsilon$  is the porosity of the sorption material in the cylindrical packed bed,  $\rho_{sl}$  is the salt density,  $\nu$  is the reaction stoichiometric coefficient (Eq. (3.2)),  $M_{sl}$  is the salt molar mass, and  $V_{STES,unit}$  is the volume of one

STES unit. To estimate the electricity consumption required by the fan to drive the airflow through the porous cylindrical STES unit, the Ergun equation is used to estimate the pressure losses ( $\Delta p_{STES,unit}$ ) and subsequently the fan consumption ( $P_{fan,unit}$ ). A radial fan with a constant efficiency ( $\eta_{fan}$ ) of 70% is assumed [45] (Eqs. (3.21)–(3.22)).

$$\frac{\Delta p_{STES,unit}}{L_{STES,unit}} = \left( \frac{\alpha \rho_a (1 - \varepsilon)}{d_p \varepsilon^3} |u_a|^2 + \frac{\beta \mu_a (1 - \varepsilon)^2}{d_p^2 \varepsilon^3} |u_a| \right) \quad (3.21)$$

$$P_{fan,unit} = \frac{\dot{m}_a \Delta p_{STES}}{\rho_a \eta_{fan}} \quad (3.22)$$

Here, the parameters  $\alpha$  and  $\beta$  are determined according to Cheng et al. [46],  $\rho_a$  is the air density,  $\mu_a$  the air viscosity,  $d_p$  the particle diameter of the sorption material,  $u_a$  the superficial air velocity in the STES unit and  $L_{STES,unit}$  the axial length of one STES unit.

From the economic perspective, the annual fixed STES cost ( $C_{STES,fix}$ ) is calculated with Eqs. (3.23)–(3.24), in which an annuity factor ( $AF$ ) is taken into account.

$$C_{STES,fix} = N_{STES,tot} E_{STES,unit} C_{STES,cap} AF \quad (3.23)$$

$$AF = \frac{IR}{1 - (1 + IR)^{-lt_{STES}}} \quad (3.24)$$

Here,  $N_{STES,tot}$  is the total amount of STES units,  $C_{STES,cap}$  is the storage capacity cost,  $IR$  is the interest rate and  $lt_{STES}$  is the STES operational lifetime.

The fixed reference cost of the STES system used in this analysis was 2.5 €/kWh<sub>cap</sub> corresponding roughly to 0.4 €/kg of active material. However, this value would include only the active material costs, and it assumes an inexpensive material [47]. The cost of a full system will be higher, and it includes also the auxiliary materials and components of the storage such as the reactor costs in which the active material is contained, the fan cost, and the various heat exchangers. Due to the relatively low technology readiness level (TRL) of this storage technology, an exact prediction of these costs in terms of €/kWh<sub>cap</sub> is not possible. However, this cost can be varied to understand what is the approximate value of the maximum cost that makes the installation of the STES economically viable. Several material and STES parameters are assumed for the optimization model, and they are listed in Table 3-1. The reactor geometrical parameters ( $D_{STES,unit}$ ,  $L_{STES,unit}$ ) have been selected so that the single STES unit volume would be approximately 50 L, a volume comparable to a prototype developed in van Alebeek et al. [48]. The sorption material density  $\rho_{sl}$  [49] and the packed bed porosity  $\varepsilon$  are assumed by considering the material in hydrated state. The selected airflow velocity in the packed bed is similar to the one used in Gaeni et al. [50].

**Table 3-1**

Main parameters for the heating grid (HG), low temperature district heating network (DHN), sorption thermal energy storage (STES), and the airflow in the STES.

Parameter	Value	Units	Parameter	Value	Units
<b>STES</b>			<b>HG</b>		
$\rho_{sl}$	2400	kg/m <sup>3</sup>	$T_{HG,sp}$	114	°C
$\Delta H_{reac}$	63.6	kJ/mol <sub>H<sub>2</sub>O</sub>	$T_{HG,rt}$	70	°C
$\Delta S_{reac}$	155	J/(mol <sub>H<sub>2</sub>O</sub> · K)	$\dot{m}_{HG}$	161	kg/s
$M_{sl}$	0.165	kg/mol	<b>DHN</b>		
$d_p$	2.5	mm	$T_{DHN,sp}$	55	°C
$C_{STES,cap}$	2.5	€/kWh <sub>cap</sub>	$T_{DHN,rt}$	30	°C
$L_{STES,unit}$	0.5	m	<b>STES Airflow</b>		
$D_{STES,unit}$	0.35	m	$u_a$	0.26	m/s
$lt_{STES}$	20	years	$\rho_a$	1.2	kg/m <sup>3</sup>
$IR$	3	%	$c_{pa}$	1004	J/(kg·K)
$\varepsilon$	0.5	–			
$\varepsilon_{HR}$	0.9	–			

## 4. Optimization framework

In this section, the reference energy system and the market mechanisms described in Sections 2 and 3 are formulated as a MILP optimization problem. Then, the scenarios in Section 2.3 are investigated and the STES size and the system operational behavior are optimized with the aim of maximizing the yearly system profit. The structure of the optimization problem consists of an objective function, containing the optimization variables, to be minimized while respecting a series of optimization constraints. The objective function in this work aims at maximizing the overall system profits while the optimization constraints describe the techno-economic behavior of the system components and the market mechanisms. Within this work, the optimization variables are written in bold while known parameters and constants are given in plain text. The optimization temporal domain ( $t_{sim}$ ) consists of one year of operation with a bi-hourly timestep ( $\Delta t = 2$  h). A year simulation with an hourly resolution has been found too computationally expensive for the investigated model. With the bi-hourly resolution, a single optimization could take up to 6 h with a machine consisting of an Intel® Core™ i7-7820HQ and 32 Gb of RAM. With a hourly resolution, the time required for a single simulation would generally increase exponentially [51]. The electricity price signals of the energy markets and the DHN demand, with an hourly resolution, have been averaged accordingly. Moreover, the periodicity of the time domain is imposed at the domain boundaries i.e.  $\{t_1, \dots, t_{end}, t_1, \dots, t_{end}, t_1\}$ . In this way, the STES state of charge ( $SOC_{STES,t}$ ) depending on its own value at the previous timestep can be represented with a yearly cyclic behavior (i.e.  $SOC_{STES,t_{sim}+1} = SOC_{STES,1}$ ). The optimization model has been solved using MATLAB© as modeling environment, Gurobi [52] as solver, and YALMIP [53] as interface between the solver and the modeling environment.

### 4.1. Optimization variables

The main variables solved in the optimization model and their domain boundaries are displayed in Table 4-1. Continuous variables can have any value within their domain; integer variables can have only integers within their domain; and semi-continuous variables can take a value of zero or any value within a domain that has both lower and upper bounds in the positive numbers domain.

The revenues variables can take positive numbers and they can be revenues from the DAM ( $R_{DAM,t}$ ) and STOR ( $R_{STOR,t}$ ) market calculated at every timestep of the temporal domain  $t_{sim}$  or they can be the revenues from the capacity market CM ( $R_{CM}$ ) that are independent of the time domain but depend only on the ORC power allocated during the CM-event.

The cost variables  $C_t$  consider only the operational costs of the STES fan. The fixed STES cost  $C_{STES,fix}$  is a parameter known a priori and based on the total number of storage units  $N_{STES,tot}$  for a specific simulation.

The ORC mass flow fraction  $f_{ORC,t}$  is a semi-continuous optimization variable defined at every timestep that can take the value of zero or a number between the minimum ORC mass flow fraction and 1. The other mass flow fraction variables ( $f_{DHN,t}$ ,  $f_{STES,t}$ , and  $f_{Res,t}$ ) can take any value from 0 to 1. The residual mass flow fraction ( $f_{Res,t}$ ) is defined in order to relax the optimization problem and track the amount of the main heating grid flow that the optimizer might not allocate to any of the three consumers. Its role is explained in more detail in Section 4.2.

The optimization variables for the electrical power at every moment in time ( $P_t$ ) track four different quantities defined in the set  $\{ORC, DAM, STOR, fan\}$ , at every moment in time.  $P_{ORC,t}$  is the power produced by the ORC, which is then divided into the power allocated to each market ( $P_{DAM,t}$  and  $P_{STOR,t}$ ).  $P_{fan,t}$  is the power required by the STES fan for the STES charging or discharging process. The thermal power discharged from the STES for the DHN demand is defined as  $P_{STES-s,t}$  and it is defined in the negative domain representing the energy

**Table 4-1**

Main optimization variable types, and validity domains. Variable types: C = continuous; I = integer; SC = semi-continuous.

Optimization variable	Type	Boundaries	Domain	Units
$R_{CM}$	C	$[0, +inf)$	$\{CM\}$	€
$R_{DAM/STOR,t}$	C	$[0, +inf)$	$\{DAM, STOR\}, t_{sim}$	€
$C_t$	C	$[0, +inf)$	$t_{sim}$	€
$f_{ORC,t}$	SC	$\{0, [f_{ORC,min}, 1]\}$	$t_{sim}$	-
$f_{DHN/STES/Res,t}$	C	$[0, 1]$	$t_{sim}$	-
$P_{ORC/DAM/STOR/fan,t}$	C	$[0, +inf)$	$\{ORC, DAM, STOR, fan\}, t_{sim}$	MW
$P_{STES-d,t}$	C	$[0, +inf)$	$t_{sim}$	MW
$P_{STES-s,t}$	C	$[-inf, 0)$	$t_{sim}$	MW
$N_{STES,t}$	I	$[-N_{STES,tot}, N_{STES,tot}]$	$t_{sim}$	-
$SO_{CSTES,t}$	C	$[0, 1]$	$t_{sim}$	-

extracted from the STES. Conversely, the STES charging power required from the main heating grid ( $P_{STES-d,t}$ ) is defined in the positive domain.

The number of STES units active at every moment in time  $N_{STES,t}$ , either during the STES charge ( $N_{STES} > 0$ ) or the STES discharge ( $N_{STES} < 0$ ), are integer variables defined in the temporal domain. Therefore, a negative value of  $N_{STES,t}$  implies that the STES is discharging  $N_{STES,t}$  units (sorption), and a positive  $N_{STES,t}$  value implies that the STES is charging  $N_{STES,t}$  units (desorption).

Finally, the STES state of charge ( $SO_{CSTES,t}$ ) is defined as a continuous variable ranging from 0 to 1 at every moment in time.

#### 4.2. Objective function and optimization constraints

The objective function  $z$  in the optimization problem aims at maximizing the overall profits of the investigated scenario over the simulated timeframe. It can be written as:

$$\min z = C_{STES,fix} - R_{CM} + \sum_{t=1}^{t_{sim}} (C_t - R_t) \quad \forall t \quad (4.1)$$

where  $C_t$  and  $R_t$  are the energy systems costs and revenues at time  $t$ , respectively.

The optimization constraints describing the operational behavior of the different system components and the markets dynamics are described.

The energy system costs taken into account in this work consist of the fixed and operational costs of the STES, the latter defined as in Eq. (4.2).  $C_t$  represents the cost of the energy ( $P_{fan,t}\Delta t$ ) used by the fan to drive the airflow.

$$C_t = P_{fan,t}\Delta t P_{DAM,t} \quad \forall t \quad (4.2)$$

The revenues are defined according to Eqs. (4.3) and (4.4), and they are representing the profits generated by selling the electricity produced from the ORC to the different markets. In particular, Eq. (4.3) represents the revenues from the capacity market, calculated as the power allocated during the CM-event ( $P_{CM}$ ) multiplied by the CM price  $p_{CM}$  expressed in €/ (MW·h).

$$R_{CM} = P_{CM} p_{CM} \quad (4.3)$$

$$R_t = \sum_{k=\{DAM,STOR\}} P_{k,t}\Delta t P_{k,t} \quad \forall t \quad (4.4)$$

The net electrical power of the ORC is estimated with the performance maps generated with an off-design ORC model (see Section 3.3). Being a deterministic model, the ambient conditions are known *a priori* for the whole simulation temporal domain  $t_{sim}$ . Therefore, only the mass flow fraction from the heating grid to the ORC evaporator  $f_{ORC,t}$  is an optimization variable. Thus, at every moment in time, the 3D-performance maps (Fig. 3.2 left) are projected into a 1D function of the mass flow fraction  $f_{ORC,t}$  (Fig. 3.2 right). This nonlinear relationship has been approximated with piecewise linear functions, which can be implemented into the MILP modeling framework [54]. In particular, for given ambient conditions, the resulting 1D-performance map of output

power versus flowrate (Fig. 3.2, right) is divided into 4 linear segments for every time step. The number of linear segments is a compromise between accuracy and computational cost. A higher resolution (i.e. a higher number of segments) would have caused a too computationally expensive model due to the high amount of additional integer variables required. A constraint (Eq. (4.5)) is used to impose that the electrical power produced by the ORC has to be equal to the one delivered to the markets, and equal or greater than the one delivered during the CM-event (Eq. (4.6)).  $P_{CM}$  is a sparse vector in which the only nonzero elements are those at timesteps where the CM-event is imposed.

$$P_{ORC,t} = \sum_{k=\{DAM,STOR\}} P_{k,t} \quad \forall t \quad (4.5)$$

$$P_{ORC,t} \geq P_{CM,t} \quad \forall t \quad (4.6)$$

The DHN thermal energy balance is imposed with Eq. (4.7). It implies that the thermal energy supplied by the main heating grid HG through the mass flow fraction  $f_{DHN,t}$ , and the one from the sorption reactor discharge are equal to the total thermal energy demand from the dwellings. It is remarked that, in Eq. (4.7),  $P_{STES-s,t}$  has negative values according to its definition.

$$f_{DHN,t} \dot{m}_{HG} c_{p,w} (T_{HG,sp} - T_{HG,rt}) - P_{STES-s,t} \eta_{STES-s,t} = P_{DHN,t} \quad \forall t \quad (4.7)$$

The mass balance of the main heating grid is defined in Eq. (4.8). It implies that the sum of the mass flow fractions directed towards the DHN, ORC, STES, and the residual mass flow fraction ( $f_{Res}$ ) are equal to one at every moment in time.

$$f_{DHN,t} + f_{ORC,t} + f_{STES,t} + f_{Res,t} = 1 \quad \forall t \quad (4.8)$$

The objective function displayed in Eq. (4.1) is minimized when all the thermal energy from the main heating grid is allocated at every moment in time. However, there can be moments in time in which this is not possible, and a relatively small amount of energy cannot be allocated. In particular, the energy from the main heating grid cannot be completely allocated when, at the same moment, the STES is fully charged, the DHN demand is not requiring more energy than what the main heating grid is already delivering, and the mass flow fraction directed towards the ORC would be lower than the minimum mass flow allowed for the ORC to work. Without the relaxing variable  $f_{Res}$ , the equality in 4.8 can lead to an unfeasible optimization problem for certain timesteps. Alternatively, Eq. (4.8) can be seen also as an inequality in which the  $f_{Res,t}$  is not present and the sum of the other terms must be lower than or equal to one. In a real system, a value of  $f_{Res,t}$  larger than zero would imply that the main heating grid return temperature ( $T_{HG,rt}$ ) increases. Therefore, the magnitude of  $f_{Res,t}$  can be interpreted as a measure of which the assumption of having a fixed supply and return temperature of the main heating grid is respected.

The STES constraints define the mass flow fraction from the heating grid that is required during the STES charging (Eq. (4.9)), the STES state of charge (Eq. (4.10)), the overall discharge (Eq. (4.11)) and

charge power (Eq. (4.12)), and the STES fan power (Eq. (4.13)).

$$f_{STES,t} = \frac{P_{STES-d,t}}{\eta_{STES-d} \dot{m}_{HG} C_{pw} (T_{HG,sp} - T_{HG,rt})} \quad \forall t \quad (4.9)$$

$$SOC_{STES,t} = SOC_{STES,t-1} + \frac{(P_{STES-d,t} + P_{STES-s,t}) \Delta t}{N_{STES,tot} E_{STES,unit}} \quad \forall t \quad (4.10)$$

$$P_{STES-s,t} = \begin{cases} 0 & N_{STES,t} > 0 \\ N_{STES,t} P_{STES-s,unit,t} & N_{STES,t} \leq 0 \end{cases} \quad \forall t \quad (4.11)$$

$$P_{STES-d,t} = \begin{cases} N_{STES,t} P_{STES-d,unit,t} & N_{STES,t} \geq 0 \\ 0 & N_{STES,t} < 0 \end{cases} \quad \forall t \quad (4.12)$$

$$P_{fan,t} = |N_{STES,t}| P_{fan,unit} \quad \forall t \quad (4.13)$$

where  $SOC_{STES,t}$  and  $SOC_{STES,t-1}$  are the STES state of charge at the current and previous time, respectively, and  $\Delta t$  is the simulation timestep of 2 h. In order to formulate the optimization problem minimizing the required amount of constraints, a sign convention for  $N_{STES,t}$  is adopted, and a piecewise linear representation of the terms  $P_{STES-d,t}$ ,  $P_{STES-s,t}$ , and  $P_{fan,t}$  is made. The domain of the optimization variable  $N_{STES,t}$  has the range  $[-N_{STES,tot}, N_{STES,tot}]$ , in which negative values imply that the reactor units are discharging, and positive values imply that the reactor units are charging. Furthermore, the values of the overall charging and discharging STES powers are equal to zero for the domain side (negative or positive, respectively) in which they have no physical meaning (Fig. 4.1). For example, the STES charging power ( $P_{STES-s,t}$ ) has nonzero values in the positive domain and a value of zero in the negative domain (Eq. (4.12)). It has to be highlighted that the slopes of the two lines for  $P_{STES-s,t}$  and  $P_{STES-d,t}$  are different because  $P_{STES-s,unit,t}$  and  $P_{STES-d,unit,t}$  are calculated differently (Eqs. (3.11) and (3.17), respectively).

The optimization problem consists of minimizing the objective function (Eq. (4.1)) subject to the constraints expressed in Eqs. (4.2)–(4.13). Different optimizations are performed by varying the STES storage size (i.e. by varying  $N_{STES,tot}$ ) in order to identify the optimal STES size, with the optimal operational behavior, that maximizes the objective function.

## 5. Results

In this section, the scenarios presented in Section 2.3 are investigated for the reference energy system presented in Section 2.1 operating in the markets described in Section 2.2. In Section 5.1, a main overview of the scenarios is given through representative economic indicators. Next, every scenario that included the STES in the optimal solution is individually analyzed from Sections 5.2 to 5.4.

In order to evaluate the system performance from an economic perspective, three main indicators are selected: the relative profit increase (RPI), the normalized net present value (NNPV) and the levelized cost of storage (LCOS). The relative profit increase is defined as in

Eq. (5.1), in which  $z$  is the value of the objective function for a specific STES size (defined as in Eq. (4.1)), and  $z_{N_{STES,tot}=0}$  is the value of the objective function without the STES integrated into the energy system.

$$RPI = \frac{(z - z_{N_{STES,tot}=0})}{z_{N_{STES,tot}=0}} \quad (5.1)$$

The NPV, expressed in €, is calculated according to Eq. (5.2).

$$NPV = -N_{STES,tot} E_{STES,unit} C_{STES,cap} + \sum_{i=1}^{t_{sim}} \frac{(R_{CM} + \sum_{t=1}^{t_{sim}} (R_t - C_t))}{(1 + IR)^i} \quad (5.2)$$

Here,  $t_{sim}$  represents the overall number of timesteps in the temporal domain, the first term on the right-hand side accounts for the STES CAPEX (capital expenditure) and the second term on the right-hand side represents the yearly cashflow stream. In this term, the double summation represents the yearly cashflow streams accounted for every year of the assumed STES lifetime. For each scenario, the NPV is normalized with respect to the NPV of the solution without the STES (Eq. (5.3)).

$$NNPV = \frac{NPV}{NPV_{N_{STES,tot}=0}} \quad (5.3)$$

The levelized cost of storage is defined according to Eq. (5.1) and expressed in €/MWh.

$$LCOS = \frac{N_{STES,tot} E_{STES,unit} C_{STES,cap} + \sum_{i=1}^{t_{sim}} \left( \frac{\sum_{t=1}^{t_{sim}} (C_t)}{(1 + IR)^t} \right)}{\sum_{i=1}^{t_{sim}} \left( \frac{\sum_{t=1}^{t_{sim}} (P_{STES-s,t} \eta_{STES-s} \Delta t)}{(1 + IR)^t} \right)} \quad (5.4)$$

Here, the first and second term of the numerator represent the initial investment for the STES and the yearly STES OPEX (operating expense), respectively. The denominator represents the yearly energy delivered from the STES to the DHN. It has to be remarked that in the NPV and LCOS definition, further revenue and cost streams can be included such as fixed and variable yearly maintenance costs, decommissioning costs, taxes and subsidies. Within this analysis, the abovementioned cashflow streams are not included.

### 5.1. Results overview

For each scenario highlight (Fig. 5.1), the relative profit increase (RPI) compared to the alternative of not having a storage for the investigated number storage units  $N_{STES,tot}$  is displayed. Moreover, the storage units are also expressed in terms of storage volume, estimated by only considering the sorption material volume.

From Fig. 5.1, it is shown that for S1 the optimal solution does not include the storage. The reason is that the storage integration, even with the smallest investigated size, would have resulted in STES CAPEX and OPEX higher than the additional revenues stream generated by the

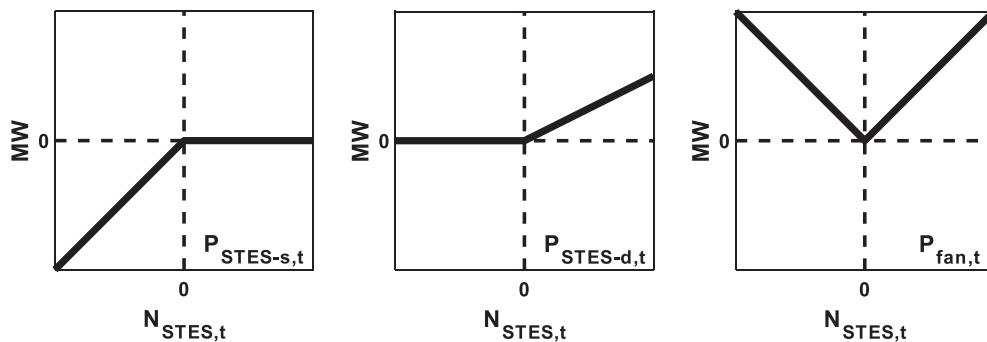


Fig. 4.1. Conceptual graph of the reactor discharging ( $P_{STES,s,t}$ ), charging ( $P_{STES,d,t}$ ), and fan ( $P_{fan,t}$ ) powers in function of the amount of active units  $N_{STES,t}$  on the left, middle, and right, respectively.

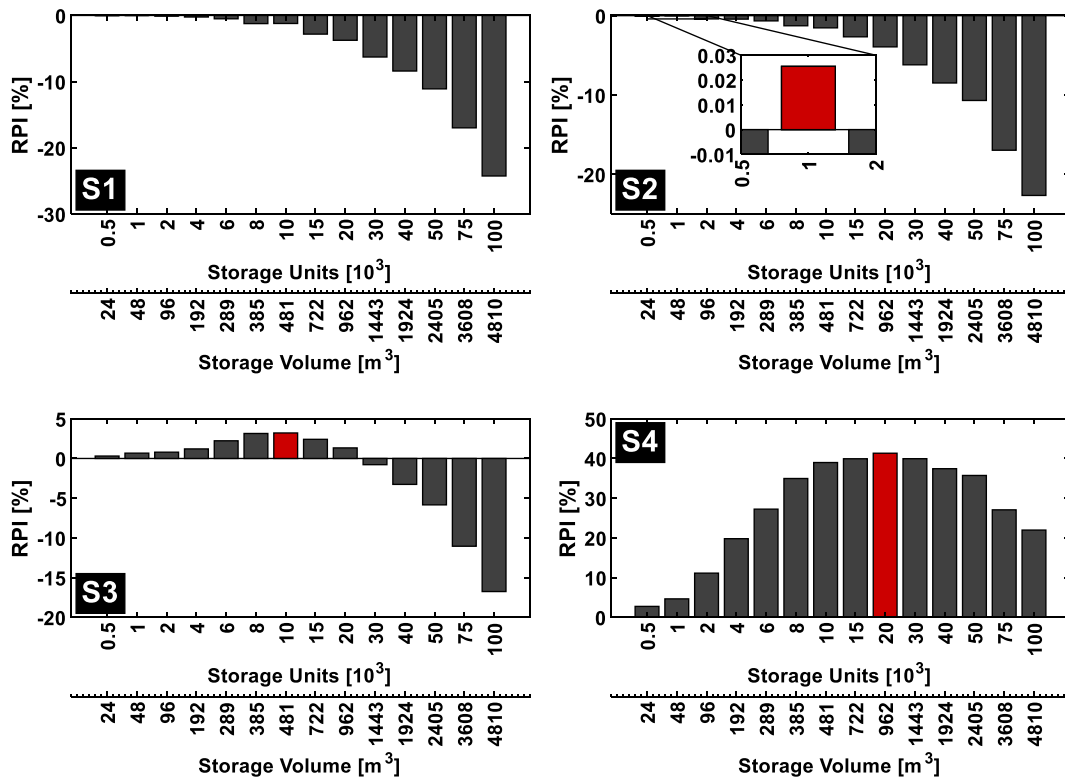


Fig. 5.1. Relative profit increase (RPI) for the investigated scenarios by varying the STES size. Top left: Scenario S1 (Belgium, DAM). Top right: Scenario S2 (UK, DAM). Bottom left: Scenario S3 (UK, DAM + CM). Bottom right: Scenario S4 (UK, DAM + CM + STOR). STES size expressed in thousands of units or m<sup>3</sup> of sorption material.

ORC thanks to the STES presence. In S2, the optimal solution includes the storage, 10<sup>3</sup> units (48 m<sup>3</sup>), but the relative profit increase of 0.03% is so small compared to the solution without the storage that it is irrelevant. On the other hand, the scenarios in the UK, in which the balancing services were active, had an increase in overall profits by the STES integration into the energy system. In scenario S3, in which the CM service is active, the inclusion of the storage up to a size of 10<sup>4</sup> units

(481 m<sup>3</sup>) increases the relative profit up to 3.2%. Finally, S4 is the scenario with the highest amount of relative profit increase (41.3%) in the optimal solution with 2·10<sup>4</sup> units (962 m<sup>3</sup>). For all scenarios, a relative profit decrease by increasing the amount of storage units means that the additional investment and operational STES costs would be higher than the revenues increase from the ORC.

Concerning the yearly amount of thermal energy delivered by the

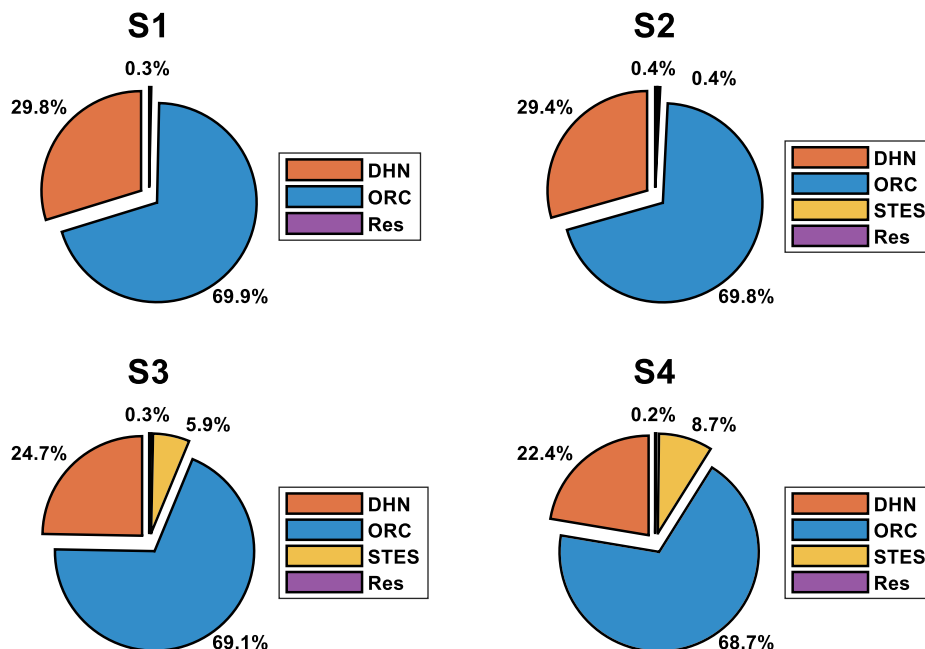


Fig. 5.2. Yearly amount of thermal energy delivered from the main heating grid to the DHN (red), ORC (blue), STES (yellow) and residual (purple) for the solution with the optimal STES size. Top left: Scenario S1. Top right: Scenario S2. Bottom left: Scenario S3. Bottom right: Scenario S4.

main heating grid (supply temperature of 114 °C) to each system component (Fig. 5.2), for S1 the fractions to the ORC and DHN are approximately 69.9% and 29.8%. For S2, the fractions were 69.8%, 29.4% and 0.4% for the STES. For S3, the overall mass flow fractions directed to the three consumers during the system yearly operation are 69.1% for the ORC, 24.7% for the DHN, and 5.9% for the storage. Finally, for S4, 8.7% of the main grid energy is delivered to the STES, 68.7% to the ORC, and 22.4% to the DHN. It is remarkable to notice that, for roughly the same amount of thermal energy delivered to the ORC, compared to other scenarios, the STOR balancing service coupled to the STES dramatically increases the system profits (Fig. 5.1 right). This is done by maximizing the energy produced by the ORC when the STOR market is active and providing the thermal energy to the DHN by discharging the STES as much as possible.

Finally, the normalized net present value (NNPV), levelized cost of storage (LCOS), and STES equivalent cycles for the scenarios in which the optimal solution included the STES (S2, S3, and S4) are shown in Fig. 5.3. As expected also from Fig. 5.1, the NNPV for scenario S2 is almost equal to zero, meaning that investing in the STES would not contribute positively to the overall system profits. For scenarios S3 and S4 the NNPV of the optimal solution is 3.21% and 39.32% meaning that the investment is profitable. This economic indicator is similar to the relative profit increase from Fig. 5.1. However, the difference between the two indicators arises from the discounted cashflows over the STES lifetime ( $lt_{STES}$ ) that are present in the NNPV calculation while for the relative profit increase only one year of operation is considered and part of the investment (Eq. (3.23)) is compounded into it through the annuity factor ( $AF$ ). Concerning the LCOS, scenarios S2 and S4 have similar values, 4.3 and 4.2 €/MWh, respectively, while scenario S3 had a LCOS of 3.3 €/MWh. This trend suggests that, for scenario S3, the yearly amount of energy delivered from the STES to the DHN relative to the storage installed capacity is higher compared to S2 or S4. This can be verified with Fig. 5.3 right, in which the equivalent STES cycles are calculated by making the ratio between the yearly amount of thermal energy delivered to the DHN and the STES installed capacity. The difference in equivalent cycles can be due to the fact that, in scenario S3, the STES size is optimized for the CM-event, which has a duration of 4 h. For the rest of the year, in S3, a STES size considerably larger than for scenario S2 is operating in the same DAM. The resulting STES operational behavior therefore can be different and it can have a larger impact on the final objective compared to a smaller STES.

In the following sections, the scenarios in which the STES is present in the optimal solution (S2, S3, and S4) are individually analyzed.

### 5.2. Scenario S2 – UK DAM

Scenario S2 assumes that the investigated energy system is located in the UK and that the only service available for the ORC for selling electrical energy is the day ahead market. In Fig. 5.4, the 2 h averaged price signal of the UK DAM is shown, for 2017. The highest price spike happened on May 17th. On that day, wind and solar dropped by two-thirds compared to the previous day, and several coal units had to be started up to fill the production gap [55]. Negative prices were also

present in the scenario (e.g. June 7th) caused by a combination of factors, namely a low local energy demand combined with a high renewable energy sources penetration, and must-run conditions of conventional power plants [56].

The optimal amount of STES units for the investigated energy system is  $10^3$ . However, this led to a profit increase of only 0.03% (Fig. 5.1) compared to not having the storage installed at all. Nevertheless, it is interesting to look at the techno-economical behavior of the energy system. In Fig. 5.5, the results are displayed over a representative time span of three days (2/04 – 5/04) are displayed. The ORC power produced (top right) in this period is fluctuating between 1 MW and 2 MW, approximately, and the revenues (bottom right) are varying from 50 € to 300 € every 2 h. In order to maximize  $f_{ORC}$  (top left) during the electricity price spikes (e.g. 2/04 at 18:00), the STES is discharged (middle left) in order to partially provide the DHN demand (bottom left).

In Fig. 5.6 left, it is shown that most of the energy produced from the ORC is sold at a price below the yearly average DAM price. Without having a storage, 39.06% of the energy is sold above  $\bar{p}_{DAM}$ . With the optimal number of storage units, it would be 39.5% while the maximum achieved (41.6%) coincides with the maximum amount of storage units investigated ( $100 \cdot 10^3$ ). However, having  $100 \cdot 10^3$  storage units would cause a profit decrease of  $-23\%$  (Fig. 5.1 top right) compared to not having the storage at all.

The yearly revenues generated by selling the ORC energy to the DAM market at a price above or below  $\bar{p}_{DAM}$ , for the optimal amount of storage units, are almost equally contributing to the overall amount of revenues.

### 5.3. Scenario S3 – UK DAM-CM

Scenario S3 involves an additional market service in which the ORC can operate: the capacity market (CM). S3 assumes the same price signals as scenario S2 for the DAM market. The additional revenues from the CM are proportional to the amount of energy that the ORC can provide to the network during a stressful event (CM-event). In Fig. 5.7, the techno-economic behavior of the system is shown for a period involving the CM-event, on January 5th between 12 pm and 4 pm. It is possible to see that during the event, although the DAM price is not at a relatively high peak (bottom right), all the mass flow from the main heating grid is directed towards the ORC (top left) and the DHN demand (bottom left) is provided entirely by the STES discharge (middle left).

In Fig. 5.8 left, the committed amount of ORC power during the CM-event, relative to the maximum ORC power during those environmental conditions, is shown. It is possible to see that a large increase is present especially for  $10^3$  to  $10^4$  storage units. Within this interval, the ORC committed power during the CM-event increases from 51.1% to 98.1%. A higher amount of storage units leads to a moderate improvement. For this reason, the optimal solution for S3 includes  $10^4$  storage units, and further increasing the number of units is not beneficial and indeed it leads to a relative profit decrease (Fig. 5.1 bottom left). In Fig. 5.8 right, a sensitivity analysis on the STES capacity cost is shown. The storage

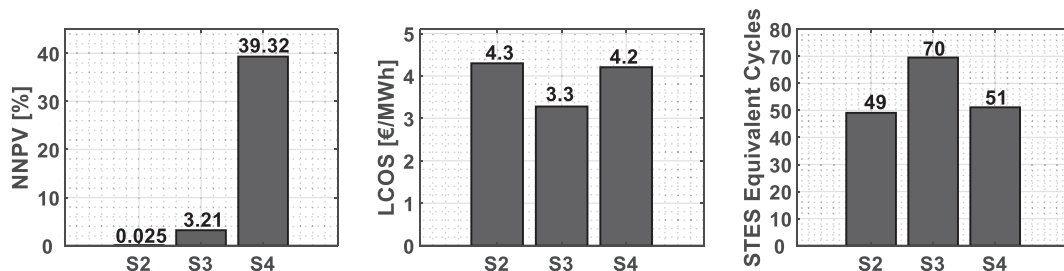


Fig. 5.3. NNPV (left), levelized cost of storage (middle), and STES equivalent cycles (right) for scenarios S2, S3, and S4 with the optimal STES size.

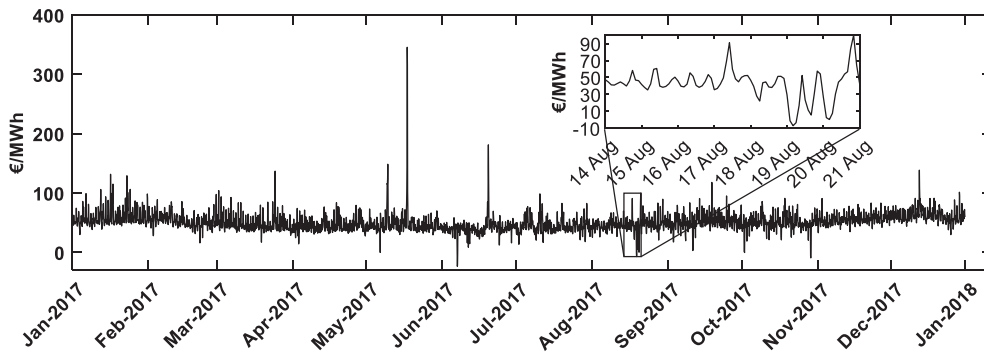


Fig. 5.4. Electricity price expressed in €/MWh for DAM. Zoomed graph between 14th of August and 21st of August.

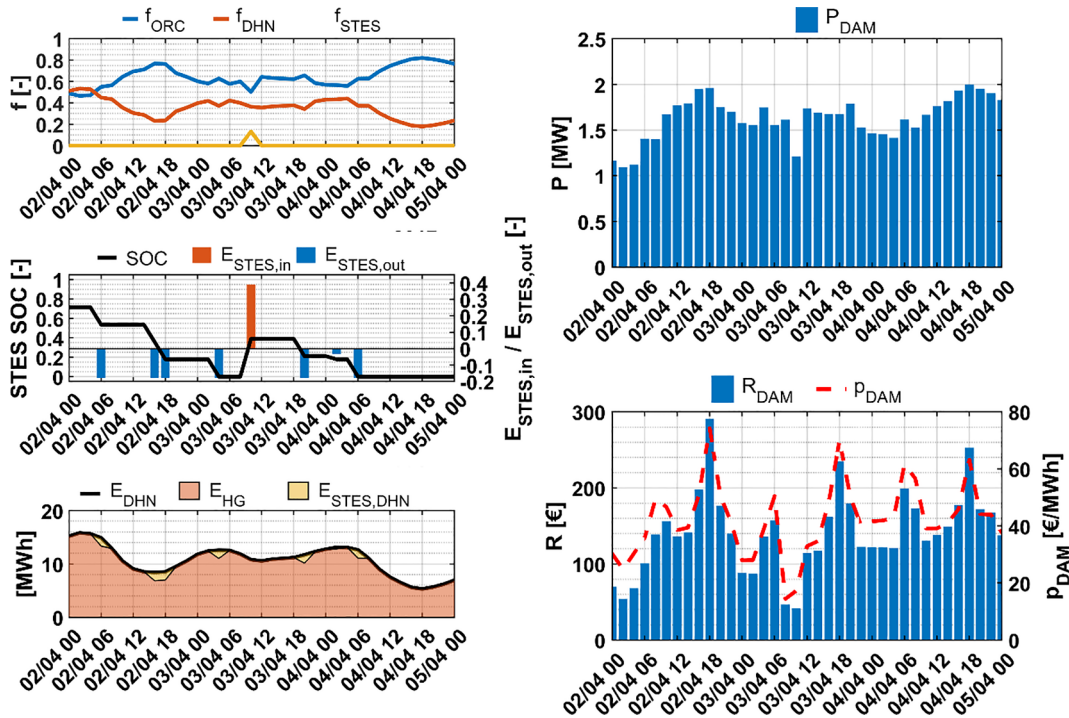


Fig. 5.5. Operational behavior of S2 over 3 days for the optimal solution ( $10^3$  STES units). Top left: mass flow fractions from the main heating grid to the district heating network ( $f_{DHN}$ ), the ORC ( $f_{ORC}$ ), and the STES ( $f_{STES}$ ). Middle left: STES state of charge (SOC) and normalized STES input ( $E_{STES,in}$ ) and output energy ( $E_{STES,out}$ ). Bottom left: District heating demand ( $E_{DHN}$ ) provided by the main heating grid ( $E_{HG}$ ) and by the STES ( $E_{STES,DHN}$ ). Top right: Electrical power produced from the ORC for the day ahead market ( $P_{DAM}$ ). Bottom right: Revenues from the day ahead market ( $R_{DAM}$ ) and day ahead market electricity price ( $P_{DAM}$ ).

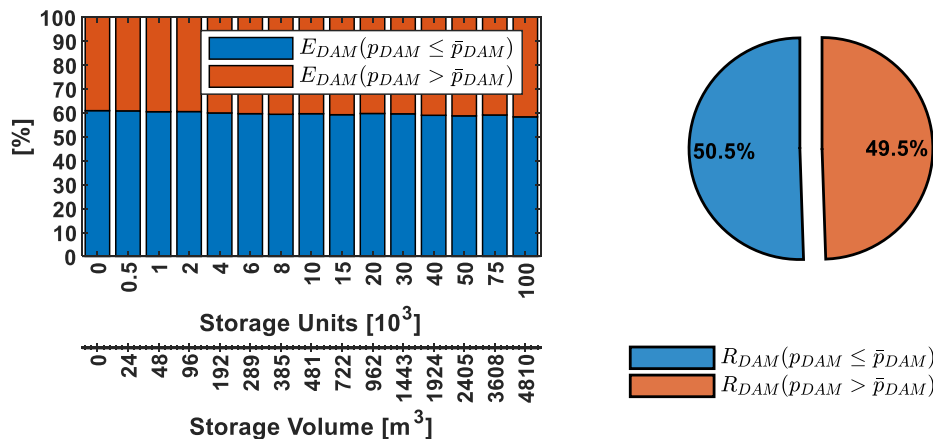


Fig. 5.6. Left: Yearly energy sold on the DAM at a price above (red) and below (blue) the yearly average market price  $\bar{p}_{DAM}$  for S2. Right: Revenues of the optimal solution ( $10^3$  STES units) for scenario S2. Red: revenues from DAM sales above  $\bar{p}_{DAM}$ . Blue: revenues from DAM sales below  $\bar{p}_{DAM}$ .

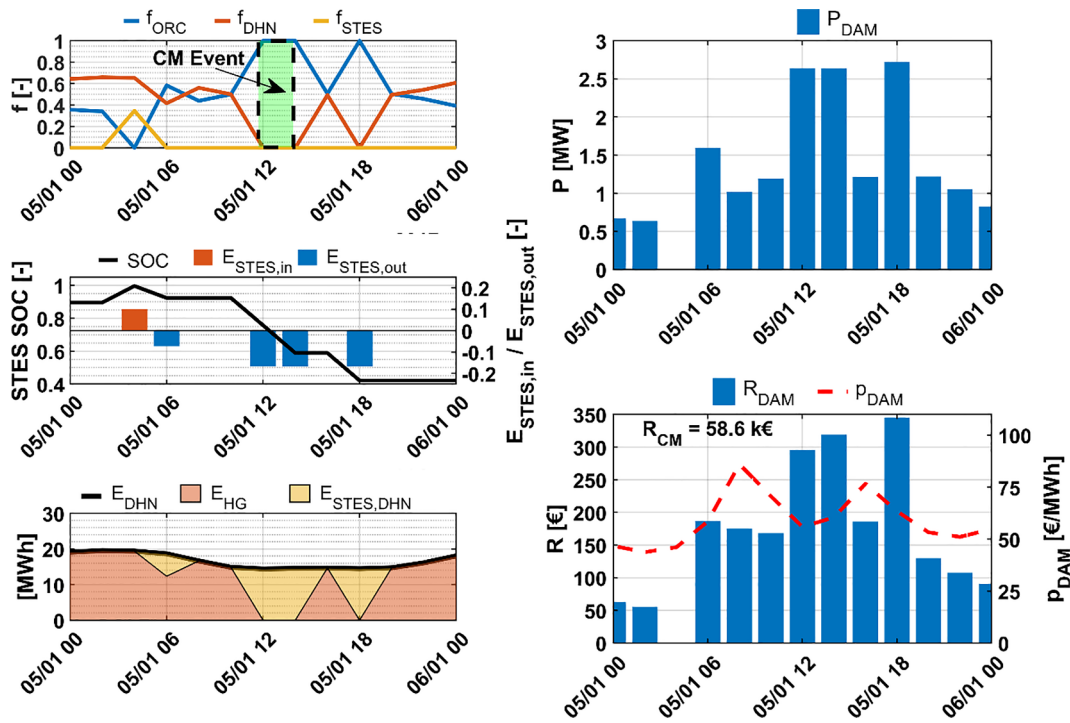


Fig. 5.7. Operational behavior of S3 for the CM event day for the optimal solution ( $10^4$  STES units). Top left: mass flow fractions from the main heating grid to the district heating network ( $f_{DHN}$ ), the ORC ( $f_{ORC}$ ), and the STES ( $f_{STES}$ ). Middle left: STES state of charge (SOC) and normalized STES input ( $E_{STES,in}$ ) and output energy ( $E_{STES,out}$ ). Bottom left: District heating demand ( $E_{DHN}$ ) provided by the main heating grid ( $E_{HG}$ ) and by the STES ( $E_{STES,DHN}$ ). Top right: Electrical power produced from the ORC for the day ahead market ( $P_{DAM}$ ). Bottom right: Revenues from the day ahead market ( $R_{DAM}$ ), CM market ( $R_{CM}$ ) and day ahead market electricity price ( $P_{DAM}$ ).

capacity cost is varied from 2.5 €/kWh<sub>cap</sub> to 12.5 €/kWh<sub>cap</sub>. The amount of STES units for each optimal solution is shown between round brackets next to the markers, and it is expressed in thousands of units. The amount of storage units in the optimal solution tends to decrease with the increase in storage capacity costs. The reason is that the profit gain due to the storage operation is not counterbalancing the increased fixed cost of the storage. Therefore, a solution with a smaller storage size becomes optimal. A storage capacity cost increase from 2.5 €/kWh<sub>cap</sub> to 5 €/kWh<sub>cap</sub> is more than halving the relative profit increase from 3.2% to 1.3%. Further increase in the capacity cost above 7.5 €/kWh<sub>cap</sub> leads the STES to be economically unfeasible.

The amount of energy sold in the DAM market above and below the yearly average price (Fig. 5.9 left) is very similar to scenario S2. The reason is that the DAM market prices are the same as in S2, and the difference relies on a market event (CM-event) of approximately 4 h,

which is only slightly influencing the yearly operational behavior of the system. For S3, the optimal solution with  $8 \cdot 10^3$  storage units, leads to an energy share sold above  $\bar{p}_{DAM}$  of 46.7%. Concerning the yearly revenues, by maximizing the ORC power produced during the CM-event led to additional revenues (Fig. 5.9 right) accounting for 8.2% of the total revenues flow. The remainder is almost equally spread between the energy sales in the DAM above and below  $\bar{p}_{DAM}$ .

#### 5.4. Scenario S4 – UK DAM-CM-STOR

In scenario S4, the STOR market is added as possible source of revenues in selling the ORC energy. The same price signals for the DAM and capacity market conditions of scenario S3 are assumed. In this scenario, the power delivered to the ORC during the STOR availability windows is maximized since the STOR utilization price is greater than

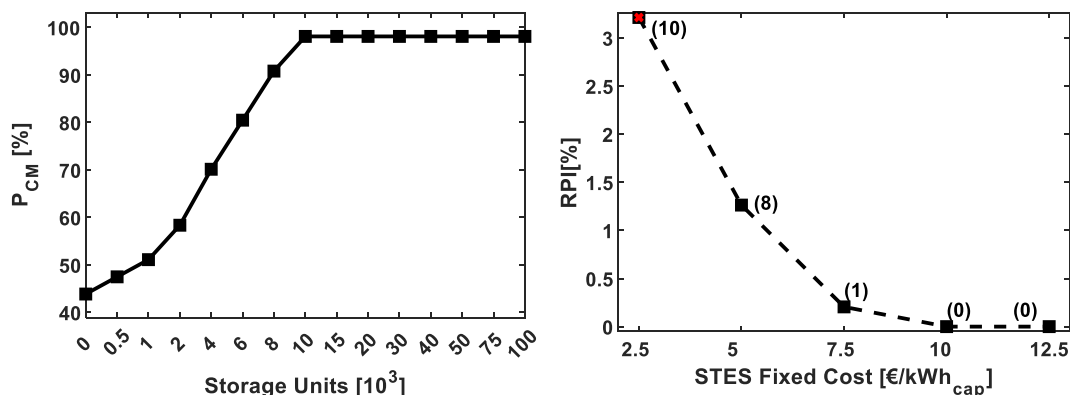


Fig. 5.8. Left: ORC power production during the CM-event ( $P_{CM}$ ) compared to the maximum producible ORC power during the CM-event. Right: Relative profit increase compared to the alternative of not having a storage for the optimal solutions in function of the fixed STES cost for S3. The amount of storage units in every optimal solution is expressed, between round brackets, in thousands of units. Red marker: Initial reference value.

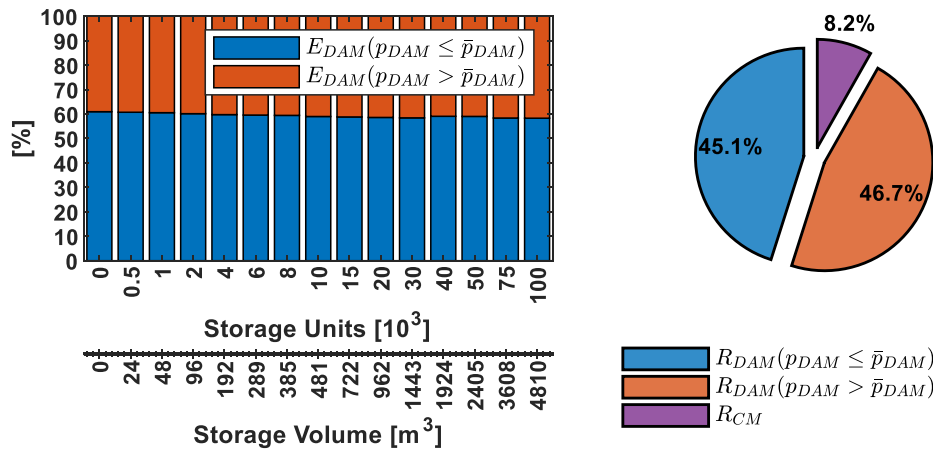


Fig. 5.9. Left: Yearly energy sold on the DAM at a price above (red) and below (blue) the yearly average market price  $\bar{p}_{DAM}$  for S3. Right: Revenues of the optimal solution ( $10^4$  STES units) for scenario S3. Red: revenues from DAM sales above  $\bar{p}_{DAM}$ . Blue: revenues from DAM sales below  $\bar{p}_{DAM}$ . Purple: revenues from the capacity market.

the average DAM price. Therefore, operating as much as possible in this market is convenient for the energy system. In Fig. 5.10 left, the operational behavior of the system is shown. On the top left it is shown how, during the STOR windows, the mass flow from the main heating grid is mostly directed towards the ORC and the DHN demand is supplied partially or totally by the STES (bottom left). Outside the STOR availability windows and when  $\bar{p}_{DAM}$  is relatively low, the system charges the STES (e.g. 31/03 at 00:00). In Fig. 5.10 top right, the ORC power sold to the STOR market (red) or to the DAM (blue) is shown. It is shown that the power sold to the STOR is constant through the same STOR season. In particular, in Fig. 5.10 bottom right, it is possible to see that the STOR season changes from season 6 to season 1 on 1/04 at 00 am, and the ORC changed the committed STOR power from 2.2 MW to

1.76 MW. This has an impact on both the revenues from the plant availability received when the unit is not called to produce and on the revenues from the plant utilization.

In Fig. 5.11 left, the relative profit in function of the STES capacity cost is displayed. For the same reasons of scenario S3 (Fig. 5.8 right), the relative profit compared to the solution of not having a storage decreases by increasing the STES capacity cost. Moreover, also the optimal number of units decreases as for scenario S3. However, while for scenario S3 the STES had a positive impact on the profit up to costs of 7.5 €/kWh<sub>cap</sub>, the presence of the STOR market in this scenario allows the storage to be profitable up to a cost of approximately 70 €/kWh<sub>cap</sub>. In Fig. 5.11 right, the STOR utilization price, which is having the major impact on the STOR revenues, has been varied over a range of

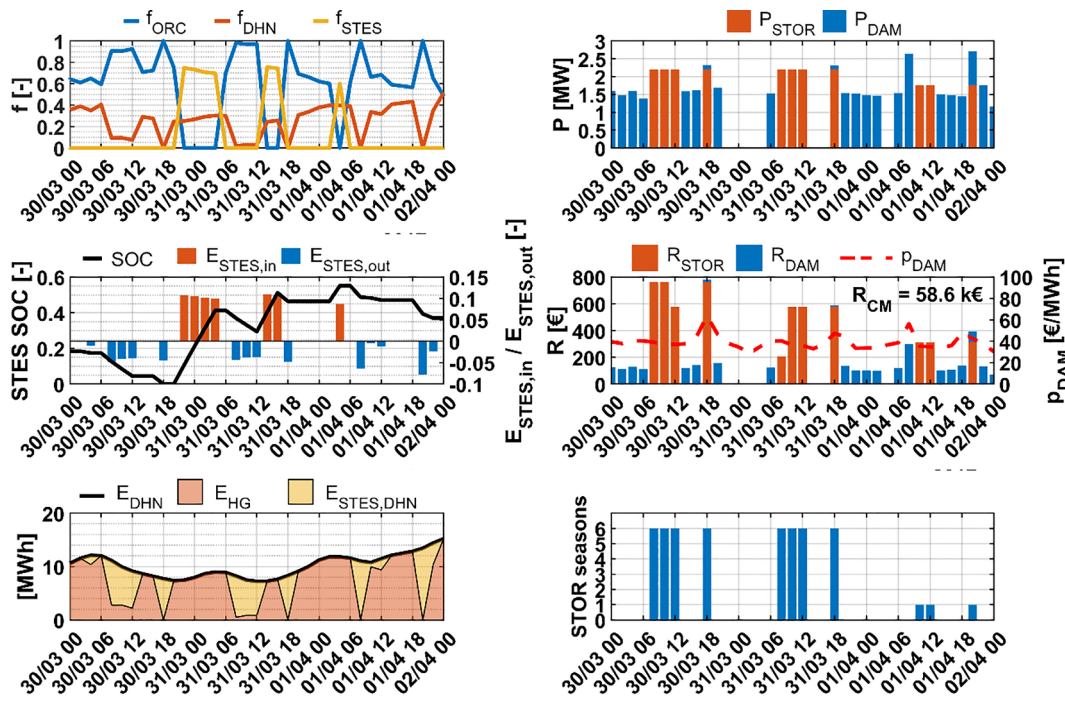


Fig. 5.10. Operational behavior of S4 over 3 days for the optimal solution ( $2 \cdot 10^4$  STES units). Top left: mass flow fractions from the main heating grid to the district heating network ( $f_{DHN}$ ), the ORC ( $f_{ORC}$ ), and the STES ( $f_{STES}$ ). Middle left: STES state of charge (SOC) and normalized STES input ( $E_{STES,in}$ ) and output energy ( $E_{STES,out}$ ). Bottom left: District heating demand ( $E_{DHN}$ ) provided by the main heating grid ( $E_{HG}$ ) and by the STES ( $E_{STES,DHN}$ ). Top right: Electrical power produced from the ORC for the day ahead market ( $P_{DAM}$ ) and for the STOR market ( $P_{STOR}$ ). Middle right: Revenues from the day ahead market ( $R_{DAM}$ ), the STOR market ( $R_{STOR}$ ) and CM market ( $R_{CM}$ ), and the day ahead market electricity price ( $p_{DAM}$ ). Bottom right: STOR seasons. The STOR season changes on 01/04 at 00:00 am from season 6 to season 1.

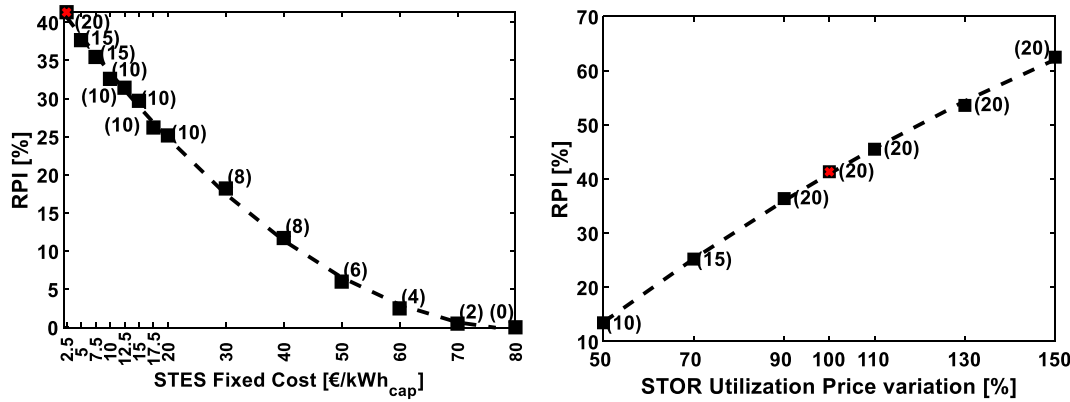


Fig. 5.11. Left: Relative profit increase compared to the alternative of not having a storage for the optimal solutions in function of the fixed STES cost for S4. Right: Relative profit increase compared to the alternative of not having a storage for the optimal solutions in function of the STOR utilization price for S4. The amount of storage units in every optimal solution is expressed, between round brackets, in thousands of units. Red markers: Initial reference values.

50–150%. The trend shows that even with a utilization price halved, a profit approximately 13.3% higher compared to not having a STES is still present. The amount of STES units in each optimal solution is decreasing for lower STOR utilization prices, as expected.

In Fig. 5.12 left, it is possible to see that the energy sold to the STOR market is increasing from approximately 17% (without STES) to 42% (with  $40 \cdot 10^3$  units). After that STES size, the amount of energy sold to the STOR market slightly decreases in favor of the energy sold on the DAM above  $\bar{p}_{DAM}$ . The optimal solution ( $2 \cdot 10^4$  units) allows 41.9% of energy to be sold to the STOR market, and 36.5% and 21.6% to be sold on the DAM market above and below  $\bar{p}_{DAM}$ , respectively. In Fig. 5.12 right, the yearly revenues flow for scenario S4 are shown. The STOR market has the highest revenues share with approximately 60.5% from the plant utilization and 2.3% from the plant commitment. The capacity market brings revenues of approximately 4.9% of the total revenues flow, and the DAM market contributes for 15.3% and 17.1% for the energy sold above and below  $\bar{p}_{DAM}$ , respectively.

Finally, a STES lifetime ( $l_{STES}$ ) of 20 years has been assumed (Table 3-1) also based on the good cyclability properties of the sorption material assumed in this work. However, in a real system, the sorption material or other system components might have to be replaced more often, thereby increasing the STES fixed cost. In Fig. 5.13, the relative profit increase of the optimal solution for different STES storage capacity costs and STES lifetime is shown. As expected, by increasing the STES capacity cost, the STES lifetime impacts more on the relative profit increase, and the number of STES units in the optimal solution

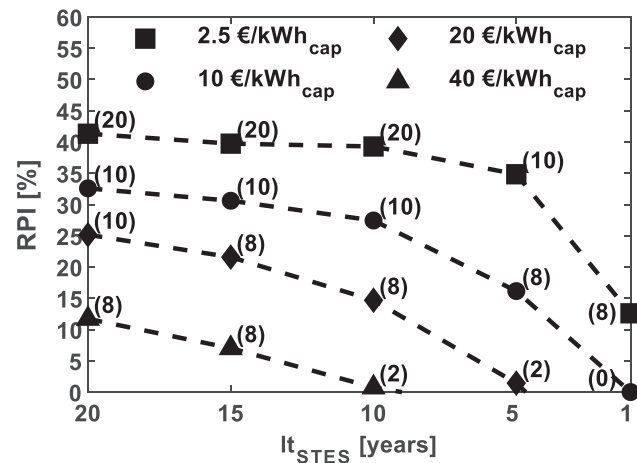


Fig. 5.13. Relative profit increase compared to the alternative of not having a storage for the optimal solutions in function of the expected STES lifetime and the fixed STES cost for S4. The amount of storage units in every optimal solution is expressed, between round brackets, in thousands of units.

decreases as well. Assuming an inexpensive material with a STES fixed cost of 2.5 €/kWh<sub>cap</sub>, the STES lifetime heavily affects the relative profit increase if it is shorter than 5 years, with the profit decreasing from 35% to 13%. Assuming a STES fixed cost of 40 €/kWh<sub>cap</sub>, halving the

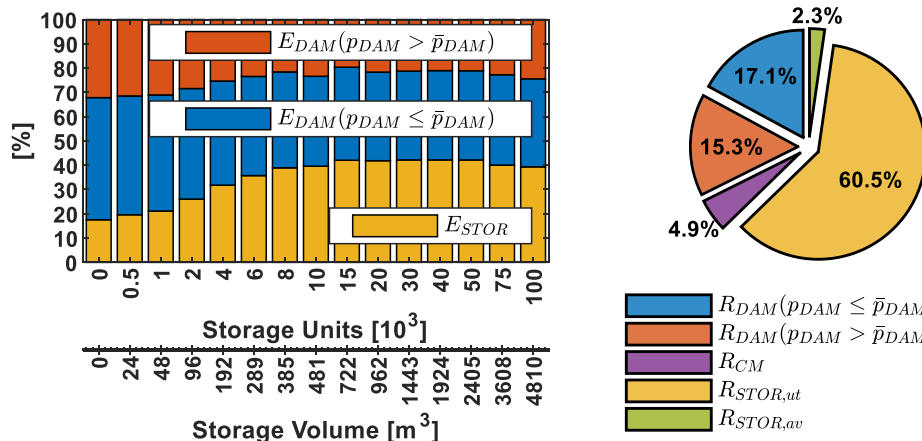


Fig. 5.12. Left: Yearly energy sold on the STOR market (yellow), and on the DAM at a price above (red) and below (blue) the yearly average market price  $\bar{p}_{DAM}$  for scenario S4. Right: Revenues of the optimal solution ( $2 \cdot 10^4$  STES units) for scenario S4. Red: revenues from DAM sales above  $\bar{p}_{DAM}$ . Blue: revenues from DAM sales below  $\bar{p}_{DAM}$ . Purple: revenues from the capacity market. Green: Revenues from committing the ORC plant to the STOR market. Yellow: Revenues from selling the energy to the STOR market.

STES lifetime would make the STES unprofitable.

## 6. Discussion and conclusions

### 6.1. Discussion on main assumptions and parameters choice

The techno-economic analysis performed in this work has intrinsic limitations due to the assumptions and parameters choices that have been made. From the STES perspective, the sorption material properties used in this work are those of potassium carbonate, which has been identified as a possible candidate for STES. In a real system, the actual sorption material performance at system-scale (e.g. degradation, kinetics, stability and cyclability) can directly affect the outcomes in terms of STES lifetime, charging and discharging power, and energy density. Moreover, the choice of a different sorption material can lead to different outcomes especially if the resulting STES energy density and fixed capacity costs are far from those of potassium carbonate. A STES lifetime ( $l_{STES}$ ) of 20 years has been assumed. However, this will effectively depend on, among other factors, the material stability and degradation over time. A shorter system lifetime would increase the yearly STES investment cost (Eq. (3.23)) and will negatively impact on the relative profit increase (Fig. 5.13). Moreover, no thermal losses have been assumed in the STES. In a real system, part of the charging and discharging STES energy is lost due to thermal losses.

The STES fan and the heat recovery unit (HR) efficiencies have been selected based on typical nominal values and are assumed constant. However, these quantities are not normally fixed and vary according to the system operating conditions. From the economic perspective, this analysis has been done by considering the electricity markets for two specific years from two specific countries. Therefore, the conclusions of this analysis are bounded to the economic frameworks in which they have been carried out. Moreover, the time resolution of the optimization model is 2 h. Finer resolutions (i.e. hourly or every 15 min) can give more accurate insights on the overall system profits since eventual local price spikes are averaged over the time intervals. However, the computational costs of the model would increase exponentially.

Concerning the component dynamics, in this work it is assumed that a steady behavior is present for each component within a single time-step ( $\Delta t = 2$  h). However, in real systems, the individual component dynamics have an influence on the results, and they should be investigated with more detailed dynamic system simulations.

Regarding the CM market, the CM-event has been arbitrarily placed in a specific period of the year, in winter, in which the DHN demand is relatively high. The CM-event location will have an impact on the RPI for a specific STES size. If, for example, a CM-event would happen in summer, it is probable that a smaller STES could maximize the system profits because the DHN demand would be lower and the ORC could already use most of the main heating grid mass flow. However, by placing the CM-event in winter, a worst-case scenario for the STES size is considered. Therefore, the yearly committed ORC capacity to the CM market could be guaranteed through the whole year with this approach. Finally, the STOR profile has been produced based on a probability-based approach. Further investigations involving multiple STOR profiles produced with the same approach should be performed to investigate the sensitivity of the STOR profile on the system profits.

### 6.2. Conclusions

The integration of a sorption thermal energy storage (STES) in an energy system operating in different energy markets has been investigated. The energy system consists of a main heating grid supplying thermal energy to a low temperature district heating network (DHN) and an organic Rankine cycle (ORC). The impact of integrating a STES in different scenarios, with the aim of maximizing the overall energy system profits, has been investigated.

It has been found that the STES integration is not profitable for

scenarios operating only in traditional markets such as the day ahead market, for the investigated day ahead market profiles (i.e. 2013 for Belgium and 2017 for UK). For the Belgian case (S1), the optimal solution did not include the STES, meaning that the STES CAPEX and OPEX were higher than the additional revenue stream generated by the ORC due to a higher flexibility provided by the STES. For the scenario in UK (S2), the STES was included in the optimal solution but it did not bring substantial additional profits, i.e. the CAPEX and OPEX were barely counterbalanced by the additional revenue stream.

When balancing services were also considered into the reference energy system, the STES integration becomes a profitable alternative. The STES presence allows for roughly 3.2% higher normalized net present value (NNPV) when the capacity market was included as market mechanism (S3). In particular, the STES allows the ORC to commit 98% of its producible power during a CM-event compared to 43.9% without STES. In turn, this led to a more than doubled revenue stream from this market mechanism.

Finally, by adding also the STOR (short term operating reserve) market as a balancing service (S4), the STES integration allowed for approximately 39% higher NNPV, which resulted from the maximization of the ORC energy produced for the STOR market. A sensitivity analysis on the STES capacity cost showed that, especially for S4, the storage integration was profitable up to a STES capacity cost of 70 €/kWh<sub>cap</sub>. Finally, an additional sensitivity analysis on the STOR utilization price, causing the major part of the revenue streams, has been performed. The results showed that even by halving the STOR utilization price, the STES integration would have led to approximately 13.3% higher profits in scenario S4.

To conclude, it is clear that the presence of balancing market mechanisms could greatly increase the commercial viability of a thermal storage technology such as sorption thermal energy storage for the reference energy system investigated in this work. Future research should investigate and compare other possible storage technologies and their impact on similar energy systems, considering the economic framework in which these systems are operating. Thus, valuable insights on the economic viability of these technologies, also still in an early development stage, can be obtained. Then, policies and guidelines can be developed to foster their integration in the future energy networks.

### Declaration of Competing Interest

The authors declare that they have no known competing financial interests or personal relationships that could have appeared to influence the work reported in this paper.

### Acknowledgments

This project receives the support of the European Union, the European Regional Development Fund ERDF, Flanders Innovation & Entrepreneurship and the Province of Limburg. TU/e has received funding from European Union's Horizon 2020 research and innovation programme under grant agreement No 657466 (INPATH-TES). The results of this study can contribute to the development of educational material within INPATH-TES. Dr. A. Sciacovelli acknowledges the finance support from Engineering and Physical Sciences Research (EPSRC) Council, UK (EP/R016402/1). Luca Scapino acknowledges Bram van der Heijde for his valuable help with the energy consumption data, and the InnoEnergy PhD School Programme and the European Institute of Technology (EIT) for supporting this research project.

### References

- [1] Rafiq S, Salim R, Nielsen I. Urbanization, openness, emissions and energy intensity: a study of increasingly urbanized emerging economies. *Energy Econ* 2016;56:20–8. <https://doi.org/10.1016/j.eneco.2016.02.007>.
- [2] Cook J, Nuccitelli D, Green SA, Richardson M, Winkler B, Painting R, et al.

- Quantifying the consensus on anthropogenic global warming in the scientific literature. *Environ Res Lett* 2013;7. <https://doi.org/10.1016/j.enpol.2014.06.003>.
- [3] European Commission. A Clean Planet for all. A European strategic long-term vision for a prosperous, modern, competitive and climate neutral economy. Brussels (BE): 2018.
- [4] Lapillonne B, Sebi C, Pollier K, Mairet N. Energy efficiency trends in buildings in the EU 2015.
- [5] Fleiter T, Elsland R, Rehfeldt M, Steinbach J, Reiter U, Catenazzi G, Jakob M, Rutten C, Harmsen R, Dittmann F, Rivière P, Stabat P. EU Profile of heating and cooling demand in 2015. Heat Roadmap Europe project. 2017.
- [6] IEA-ETSAP, IRENA. Thermal Energy Storage – Technology Brief. 2013.
- [7] Blarke MB, Dotzauer E. Intermittency-friendly and high-efficiency cogeneration: Operational optimisation of cogeneration with compression heat pump, flue gas heat recovery, and intermediate cold storage. *Energy* 2011;36:6867–78. <https://doi.org/10.1016/j.energy.2011.10.008>.
- [8] Amrollahi MH, Bathaee SMT. Techno-economic optimization of hybrid photovoltaic/wind generation together with energy storage system in a stand-alone micro-grid subjected to demand response. *Appl Energy* 2017;202:66–77. <https://doi.org/10.1016/j.apenergy.2017.05.116>.
- [9] Li Z, Xu Y. Optimal coordinated energy dispatch of a multi-energy microgrid in grid-connected and islanded modes. *Appl Energy* 2018;210:974–86. <https://doi.org/10.1016/j.apenergy.2017.08.197>.
- [10] Martínez Ceseña EA, Good N, Syri ALA, Mancarella P. Techno-economic and business case assessment of multi-energy microgrids with co-optimization of energy, reserve and reliability services. *Appl Energy* 2018;210:896–913. <https://doi.org/10.1016/j.apenergy.2017.08.131>.
- [11] Terlouw T, Alskaf T, Bauer C, van Sark W. Multi-objective optimization of energy arbitrage in community energy storage systems using different battery technologies. *Appl Energy* 2019;239:356–72. <https://doi.org/10.1016/j.apenergy.2019.01.227>.
- [12] Frate GF, Carro PP, Ferrari L, Desideri U. Techno-economic sizing of a battery energy storage coupled to a wind farm: an Italian case study. *Energy Procedia* 2018;148:447–54. <https://doi.org/10.1016/j.egypro.2018.08.119>.
- [13] Blarke MB, Yazawa K, Shakouri A, Carmo C. Thermal battery with CO<sub>2</sub> compression heat pump: techno-economic optimization of a high-efficiency Smart Grid option for buildings. *Energy Build* 2012;50:128–38. <https://doi.org/10.1016/j.enbuild.2012.03.029>.
- [14] McKenna R, Fehrenbach D, Merkel E. The role of seasonal thermal energy storage in increasing renewable heating shares: a techno-economic analysis for a typical residential district. *Energy Build* 2019. <https://doi.org/10.1016/j.enbuild.2019.01.044>.
- [15] Pielichowska K, Pielichowski K. Phase change materials for thermal energy storage. *Prog Mater Sci* 2014;65:67–123. <https://doi.org/10.1016/j.pmatsci.2014.03.005>.
- [16] Yu N, Wang RZ, Wang LW. Sorption thermal storage for solar energy. *Prog Energy Combust Sci* 2013;39:489–514. <https://doi.org/10.1016/j.pecs.2013.05.004> Review.
- [17] Donkers PAJ, Sögütoglu LC, Huinink HP, Fischer HR, Adan OCG. A review of salt hydrates for seasonal heat storage in domestic applications. *Appl Energy* 2017;199:45–68. <https://doi.org/10.1016/j.apenergy.2017.04.080>.
- [18] Janchen J, Schumann K, Thrun E, Brandt A, Unger B, Hellwig U. Preparation, hydrothermal stability and thermal adsorption storage properties of binderless zeolite beads. *Int J Low-Carbon Technol* 2012;1–5. <https://doi.org/10.1093/ijlct/cts037>.
- [19] Dawoud B, Aristov Y. Experimental study on the kinetics of water vapor sorption on selective water sorbents, silica gel and alumina under typical operating conditions of sorption heat pumps. *Int J Heat Mass Transf* 2003;46:273–81. [https://doi.org/10.1016/S0017-9310\(02\)00288-0](https://doi.org/10.1016/S0017-9310(02)00288-0).
- [20] Henninger SK, Schmidt FP, Henning HM. Water adsorption characteristics of novel materials for heat transformation applications. *Appl Therm Eng* 2010;30:1692–702. <https://doi.org/10.1016/j.applthermaleng.2010.03.028>.
- [21] Henninger SK, Jeremias F, Kummer H, Janiak C. MOFs for use in adsorption heat pump processes. *Eur J Inorg Chem* 2012;2625–34. <https://doi.org/10.1002/ejic.201101056>.
- [22] Scapino L, Zondag HA, Van Bael J, Diriken J, Rindt CCM. Sorption heat storage for long-term low-temperature applications: a review on the advancements at material and prototype scale. *Appl Energy* 2017;190:920–48. <https://doi.org/10.1016/j.apenergy.2016.12.148>.
- [23] N'Tsoukpoe KE, Restuccia G, Schmidt T, Py X. The size of sorbents in low pressure sorption or thermochemical energy storage processes. *Energy* 2014;77:983–98. <https://doi.org/10.1016/j.energy.2014.10.013>.
- [24] Solé A, Miró L, Barreneche C, Martorell I, Cabeza LF. Corrosion test of salt hydrates and vessel metals for thermochemical energy storage. *Energy Procedia* 2014;48:431–5. <https://doi.org/10.1016/j.egypro.2014.02.050>.
- [25] National Grid UK. Capacity (EMR and CMN) 2018. <https://www.nationalgrid.com/uk/electricity/capacity-emr-and-cmn> (accessed June 10, 2018).
- [26] National Grid. GB Electricity Capacity Market Notices 2018. <https://gbcmn.nationalgrid.co.uk/> (accessed October 25, 2018).
- [27] Ofgem. Annual Report on the Operation of the Capacity Market in 2016/17. 2017.
- [28] National Grid UK. Short term operating reserve (STOR) 2018. <https://www.nationalgrid.com/uk/electricity/balancing-services/reserve-services/short-term-operating-reserve-stor> (accessed June 10, 2018).
- [29] National Grid UK. STOR Annual Market Report 2016/17. 2017.
- [30] VITO NV. Balmatt Energy Plant 2019. <https://vito.be/en/deep-geothermal/balmatt-energy-plant> (accessed February 6, 2019).
- [31] Lund H, Werner S, Wiltshire R, Svendsen S, Thorsen JE, Hvelplund F, et al. 4th Generation District Heating (4GDH). Integrating smart thermal grids into future sustainable energy systems. *Energy* 2014;68:1–11. <https://doi.org/10.1016/j.energy.2014.02.089>.
- [32] Remmen P, Lauster M, Mans M, Fuchs M, Osterhage T, Müller D. TEASER: an open tool for urban energy modelling of building stocks. *J Build Perform Simul* 2018;11:84–98. <https://doi.org/10.1080/19401493.2017.1283539>.
- [33] De Jaeger I, Reynders G, Ma Y, Saelens D. Impact of building geometry description within district energy simulations. *Energy* 2018;158:1060–9. <https://doi.org/10.1016/j.energy.2018.06.098>.
- [34] van der Heijde B. Optimal integration of thermal energy storage and conversion in fourth generation thermal networks. 2019.
- [35] Baetens R, Saelens D. Modelling uncertainty in district energy simulations by stochastic residential occupant behaviour. *J Build Perform Simul* 2016;9:431–47. <https://doi.org/10.1080/19401493.2015.1070203>.
- [36] Wilcox S, Marion W. Users Manual for TMY3 Data Sets. Colorado: Golden; 2008.
- [37] Bell IH, Wronski J, Quoilin S, Lemort V. Pure and pseudo-pure fluid thermophysical property evaluation and the open-source thermophysical property library coolprop. *Ind Eng Chem Res* 2014;53:2498–508. <https://doi.org/10.1021/ie4033999>.
- [38] Sinnott RK. *Chemical Engineering Design*. 6th ed. Elsevier; 2005.
- [39] Scapino L, Zondag HA, Van Bael J, Diriken J, Rindt CCM. Energy density and storage capacity cost comparison of conceptual solid and liquid sorption seasonal heat storage systems for low-temperature space heating. *Renew Sustain Energy Rev* 2017;76:1314–31. <https://doi.org/10.1016/j.rser.2017.03.101>.
- [40] Sögütoglu LC, Donkers PAJ, Fischer HR, Huinink HP, Adan OCG. In-depth investigation of thermochemical performance in a heat battery: Cyclic analysis of K<sub>2</sub>CO<sub>3</sub>, MgCl<sub>2</sub> and Na<sub>2</sub>S. *Appl Energy* 2018;215:159–73. <https://doi.org/10.1016/j.apenergy.2018.01.083>.
- [41] Glasser L. Thermodynamics of inorganic hydration and of humidity control, with an extensive database of salt hydrate pairs. *J Chem Eng Data* 2014;59:526–30. <https://doi.org/10.1021/je401077x>.
- [42] Greenspan L. Humidity fixed points of binary saturated aqueous solutions. *J Res Natl Bur Stand Sect A Phys Chem* 1977;81A:89. <https://doi.org/10.6028/jres.081A.011>.
- [43] Scapino L, Zondag HA, Diriken J, Rindt CCM, Van Bael J, Sciacovelli A. Modeling the performance of a sorption thermal energy storage reactor using artificial neural networks. *Appl Energy* 2019;253:113525. <https://doi.org/10.1016/j.apenergy.2019.113525>.
- [44] Merzkirch A, Maas S, Scholzen F, Waldmann D. Field tests of centralized and decentralized ventilation units in residential buildings - Specific fan power, heat recovery efficiency, shortcuts and volume flow unbalances. *Energy Build* 2016;116:373–83. <https://doi.org/10.1016/j.enbuild.2015.12.008>.
- [45] *AMCA Fan Efficiency Standards for Commercial & Industrial Buildings*. USA: Arlington Heights; 2014.
- [46] Cheng NS. Wall effect on pressure drop in packed beds. *Powder Technol* 2011;210:261–6. <https://doi.org/10.1016/j.powtec.2011.03.026>.
- [47] Trausel F, de Jong A-J, Cuyper R. A review on the properties of salt hydrates for thermochemical storage. SHC 2013, Int. Conf. Sol. Heat. Cool. Build. Ind. Elsevier B.V.; 2014. p. 447–52. <https://doi.org/10.1016/j.egypro.2014.02.053>.
- [48] van Alebeek R, Scapino L, Beving MAJM, Gaeini M, Rindt CCM, Zondag HA. Investigation of a household-scale open sorption energy storage system based on the zeolite 13X/water reacting pair. *Appl Therm Eng* 2018;139:325–33. <https://doi.org/10.1016/j.applthermaleng.2018.04.092>.
- [49] Boreal Science. Potassium Carbonate 1.5-Hydrate 2019. <https://boreal.com/store/product/8884553/potassium-carbonate-1-5-hydrate>.
- [50] Gaeini M, Zondag HA, Rindt CCM. Effect of kinetics on the thermal performance of a sorption heat storage reactor. *Appl Therm Eng* 2016;102:520–31. <https://doi.org/10.1016/j.applthermaleng.2016.03.055>.
- [51] Till J, Engell S, Panek S, Stursberg O. Empirical Complexity Analysis of a MILP-Approach for Optimization of Hybrid Systems. IFAC Proc 2003;36:129–34. [https://doi.org/10.1016/S1474-6670\(17\)36419-4](https://doi.org/10.1016/S1474-6670(17)36419-4).
- [52] Gurobi Optimization Inc. Gurobi Optimizer Reference Manual 2017: 717.
- [53] Löfberg J. YALMIP: A Toolbox for Modeling and Optimization in MATLAB. CACSD Conf., Taipei, Taiwan; 2004.
- [54] Lin MH, Carlsson JG, Ge D, Shi J, Tsai JF. A review of piecewise linearization methods. *Math Probl Eng* 2013 2013. <https://doi.org/10.1155/2013/101376>.
- [55] Staffell I, Scurlock J. Drax Electric Insights Quarterly – Q2 2017. 2018.
- [56] Argus Media group. UK sees longest period of negative power prices 2017. <https://www.argusmedia.com/en/news/1474697-uk-sees-longest-period-of-negative-power-prices> (accessed August 7, 2019).